



2



DTIC
ELECTE
JAN 31 1992
S B D

AN INVESTIGATION OF THE INTERATOMIC BONDING CHARACTERISTICS OF A Ti - 51at.% Al ALLOY BY X-RAY DIFFRACTION

June, 1991

Alan G. Fox

Approved for public release; distribution is unlimited.

92-02431



0-7-8

REPORT DOCUMENTATION PAGE												
1a. REPORT SECURITY CLASSIFICATION UNCLASSIFIED			1b. RESTRICTIVE MARKINGS									
2a. SECURITY CLASSIFICATION AUTHORITY			3. DISTRIBUTION/AVAILABILITY OF REPORT Approved for public release; distribution is unlimited.									
2b. DECLASSIFICATION/DOWNGRADING SCHEDULE												
4. PERFORMING ORGANIZATION REPORT NUMBER(S)			5. MONITORING ORGANIZATION REPORT NUMBER(S)									
6a. NAME OF PERFORMING ORGANIZATION Naval Postgraduate School		6b. OFFICE SYMBOL (If applicable) ME	7a. NAME OF MONITORING ORGANIZATION Naval Postgraduate School									
6c. ADDRESS (City, State, and ZIP Code) Monterey, CA 93943-5000			7b. ADDRESS (City, State, and ZIP Code) Monterey, CA 93943-5000									
8a. NAME OF FUNDING/SPONSORING ORGANIZATION		8b. OFFICE SYMBOL (If applicable)	9. PROCUREMENT INSTRUMENT IDENTIFICATION NUMBER									
8c. ADDRESS (City, State, and ZIP Code)			10. SOURCE OF FUNDING NUMBERS									
			<table border="1"> <tr> <td>Program Element No.</td> <td>Project No.</td> <td>Task No.</td> <td>Work Unit Accession Number</td> </tr> <tr> <td></td> <td></td> <td></td> <td></td> </tr> </table>		Program Element No.	Project No.	Task No.	Work Unit Accession Number				
Program Element No.	Project No.	Task No.	Work Unit Accession Number									
11. TITLE (Include Security Classification) AN INVESTIGATION OF THE INTERATOMIC BONDING CHARACTERISTICS OF A Ti - 51at.% Al ALLOY BY X-RAY DIFFRACTION												
12. PERSONAL AUTHOR(S) Cade, Steven C.												
13a. TYPE OF REPORT Master's Thesis		13b. TIME COVERED From To	14. DATE OF REPORT (year, month, day) June 1991	15. PAGE COUNT 71								
16. SUPPLEMENTARY NOTATION The views expressed in this thesis are those of the author and do not reflect the official policy or position of the Department of Defense or the U.S. Government.												
17. COSATI CODES			18. SUBJECT TERMS (continue on reverse if necessary and identify by block number)									
FIELD	GROUP	SUBGROUP	X-ray Diffraction, XRD, TiAl, titanium, aluminum, bonding characteristics, titanium aluminides, Debye-Waller temperature factor, structure factor									
19. ABSTRACT (continue on reverse if necessary and identify by block number)												
<p>The lattice parameters and atomic structure factors of an homogenized, binary, Ti-51at.%Al intermetallic alloy were investigated using powder X-ray diffraction procedures. Powder samples were prepared by pulverizing in a mortar and pestle lathe turnings taken from a sample ingot. The powder was then annealed to relieve the induced stress and passed through a U.S. Standard #400 sieve mesh (38 microns). Lattice parameters of the face-centered tetragonal structure determined from XRD peak positions indicated a c/a ratio of 1.020; values of 4.077 Å and 3.997 Å were obtained for c_0 and a_0, respectively. These results are in agreement with previous research into γ-phase TiAl. Measurement of diffracted intensities was accomplished to determine the Debye-Waller temperature factor with a value of $B = 0.58 \text{ Å}^2$ obtained by the Wilson Method. A reduction in expected measured intensities was noted, particularly at lower Bragg angles. This was attributed to extinction based on the results of a powder particle size average of 24.3 microns. Despite the problems of extinction, the observed Debye-Waller factor was judged to be reasonably accurate upon comparison to characteristic temperature and melting point data of the Ti-Al system.</p>												
20. DISTRIBUTION/AVAILABILITY OF ABSTRACT <input checked="" type="checkbox"/> UNCLASSIFIED-UNLIMITED <input type="checkbox"/> SAME AS REPORT <input type="checkbox"/> DTIC USERS			21. ABSTRACT SECURITY CLASSIFICATION Unclassified									
22a. NAME OF RESPONSIBLE INDIVIDUAL Alan G. Fox			22b. TELEPHONE (Include Area code) 408-646-2142	22c. OFFICE SYMBOL ME/F's								

Approved for public release; distribution is unlimited.

An Investigation of the Interatomic Bonding
Characteristics of a Ti - 51at.% Al Alloy
by X-Ray Diffraction

by

Steven C. Cade
Lieutenant, United States Navy
B.S., United States Naval Academy, 1985

Submitted in partial fulfillment
of the requirements for the degree of

MASTER OF SCIENCE IN MECHANICAL ENGINEERING

from the

NAVAL POSTGRADUATE SCHOOL

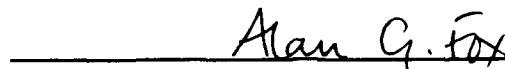
June 1991

Author:

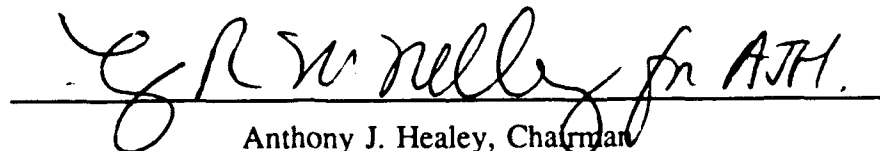


Steven C. Cade

Approved by:



Alan G. Fox, Thesis Advisor



Anthony J. Healey, Chairman

Department of Mechanical Engineering

ABSTRACT

The lattice parameters and atomic structure factors of an homogenized, binary, Ti-51at.%Al intermetallic alloy were investigated using powder X-ray diffraction procedures. Powder samples were prepared by pulverizing in a mortar and pestle lathe turnings taken from a sample ingot. The powder was then annealed to relieve the induced stress and passed through a U.S. Standard #400 sieve mesh (38 microns). Lattice parameters of the face-centered tetragonal structure determined from XRD peak positions indicated a c/a ratio of 1.020; values of 4.077\AA and 3.997\AA were obtained for c_0 and a_0 respectively. These results are in agreement with previous research into γ -phase TiAl. Measurement of diffracted integrated intensities was accomplished to determine the Debye-Waller temperature factor with a value of $B = 0.58 \text{ \AA}^2$ obtained by the Wilson Method. A reduction in expected measured intensities was noted, particularly at lower Bragg angles. This was attributed to extinction based on the results of a powder particle size average of 24.3 microns. Despite the problems of extinction, the observed Debye-Waller factor was judged to be reasonably accurate upon comparison to characteristic temperature and melting point data of the Ti-Al system.



iii

Accession For	
NTIS GRA&I	<input checked="checked" type="checkbox"/>
DTIC TAB	<input type="checkbox"/>
Unannounced	<input type="checkbox"/>
Justification	
By	
Distribution/	
Availability Codes	
Dist	Avail and/or Special
A-1	

TABLE OF CONTENTS

I. INTRODUCTION	1
II. BACKGROUND	3
A. TITANIUM-ALUMINUM ALLOYS	3
1. Development and Utilization	3
2. Current Research Emphasis	4
B. MATERIAL CHARACTERISTICS	5
1. Microstructure	5
a. γ Phase	5
b. Crystallography	8
2. Engineering Properties	9
a. Deformation Mechanisms and Ductility	9
b. Other Fracture and Embrittling Mechanisms	12
c. Impurities and Alloy Addition Effects	16
3. Methods of Analysis	19
a. X-ray Pendellösung Measurement	21
b. γ -ray Diffraction	22

c. Electron Diffraction	22
d. X-ray Diffraction	23
C. FUNDAMENTALS OF X-RAY DIFFRACTION	23
1. X-Ray Diffraction Geometry	23
2. Factors Affecting Diffracted Intensities	25
a. Atomic Structure Factor	25
b. Atomic Scattering and Dispersion	27
c. Multiplicity	28
d. Lorentz-Polarization Factor	28
e. Temperature Factor	29
f. Extinction	31
g. Preferred Orientation	32
3. Lattice Parameter Determination	33
4. Debye-Waller Factor by the Wilson Method	33
D. SCOPE OF PRESENT WORK	34
III. EXPERIMENTAL PROCEDURE	35
A. SAMPLE PREPARATION	35
B. MICROSCOPY	36
C. X-RAY DIFFRACTION	36
IV. RESULTS AND DISCUSSION	38

A. SAMPLE ANALYSIS	38
1. Observations of Microstructure	38
B. X-RAY DIFFRACTION RESULTS	38
1. Lattice Parameter Measurements	40
2. Measurement of Debye-Waller Factor	43
C. PARTICLE SIZE EXAMINATION	46
 V. CONCLUSIONS	 49
 VI. RECOMMENDATIONS	 51
 APPENDIX A. XRD REFLECTIONS AND INTEGRATED INTENSITIES	 52
 APPENDIX B. NELSON-RILEY EXTRAPOLATION DATA	 54
 APPENDIX C. WILSON PLOT DATA	 55
 LIST OF REFERENCES	 57
 INITIAL DISTRIBUTION LIST	 62

LIST OF TABLES

Table 1. PROPERTIES OF HIGH TEMPERATURE ALLOYS	10
Table 2. REFLECTION POSITIONS AND INTEGRATED INTENSITIES	52
Table 3. NELSON-RILEY EXTRAPOLATION DATA: a	54
Table 4. NELSON-RILEY EXTRAPOLATION DATA: c	54
Table 5. WILSON PLOT DATA: FUNDAMENTAL REFLECTIONS	55
Table 6. WILSON PLOT DATA: SUPERLATTICE REFLECTIONS	56

LIST OF FIGURES

Figure 1. Ti-Al Phase Diagram	6
Figure 2. Proposed Alterations to the Ti-Al Phase Diagram	7
Figure 3. $L1_0$ Lattice Structure of γ -TiAl	9
Figure 4. Possible Burgers Vectors in TiAl	11
Figure 5. Vickers Hardness vs. Composition	13
Figure 6. Partial Ti-Al Phase Diagram (Proposed) [Ref. 30, p. 428]	15
Figure 7. The Octahedral Interstitial Site in TiAl	18
Figure 8. Charge Density Contours of the DO_{19} (0001) Plane	20
Figure 9. Bragg's Law Geometry	24
Figure 10. Intensity Peak with $K\alpha_2$ Doublet	26
Figure 11. Temperature Factor of Iron at 20°C [Ref. 49, p. 136]	30
Figure 12. Intensity Deviation Due to Crystallite Size [Ref. 47, p. 367]	32
Figure 13. Optical Micrograph of Ti-51at.%Al (50X)	39
Figure 14. Nelson-Riley Extrapolations for Lattice Parameters a_0 and c_0	41
Figure 15. Lattice Parameter Comparison	42
Figure 16. Debye-Waller Determination from Fundamental Reflections	44
Figure 17. Debye-Waller Determination from Superlattice Reflections	46
Figure 18. SEM Micrograph of XRD Powder Particles (575X)	47

I. INTRODUCTION

Titanium aluminides are recognized for their high specific strength, particularly at elevated temperatures. In addition, these alloys have long received interest in the aerospace industry due to their low density and resistance to oxidation. Accordingly, a large amount of the research and development into the titanium-aluminum system has been supported by this technology sector, with applications resulting in a variety of air and spacecraft components.

While much of the focus of previous research has been centered upon Ti-Al alloys of low aluminum content, recent years have seen a greater emphasis placed on the ordered intermetallics Ti_3Al and TiAl . Substantial benefits over conventional titanium alloys have been documented in these compounds, including high temperature properties approaching those of nickel based superalloys. However, difficulties in fabrication have been encountered due to their limited ductility at low temperatures. [Ref. 1]

Considerable research has been undertaken concerning the effects on ductility of processing methods, dispersion strengthening, and alloy additions. Ternary alloying shows excellent potential but its role in reducing the inherent brittleness exhibited in Ti-Al alloys is still in question. A major portion of the research in this area has concentrated on microstructural changes and dislocation behavior resulting from the introduction of various elements, including niobium, gallium, and ruthenium, among others.

Fundamental to the understanding of the consequences of these alloy additions is a knowledge of the interatomic bonding characteristics of binary titanium aluminides. Upon the introduction of a third element to the system, a rearrangement of the valence electron distribution occurs which affects the physical properties of the material. A thorough investigation of bonding mechanisms by examination of electron charge densities may therefore provide a solution to the brittleness problem.

Accurate atomic structure factor measurements are a prerequisite to determining electron charge distributions. Various experimental and theoretical methods of analysis are available to accomplish this, including X-ray Pendellösung methods, γ -, X-ray, and electron diffraction. Excellent results for β' -NiAl have been obtained by Cooper using X-ray diffraction [Ref. 2] and by Fox and Tabbernor using the critical voltage method in electron diffraction [Ref. 3]. As well as the charge distribution the structure factors depend on the vibration of atoms about their equilibrium positions; diffracted intensities serve as an indicator of this vibrational motion through an evaluation of Debye-Waller temperature factors. This study will utilize X-ray diffraction on an homogenized, binary Ti-51at%Al alloy to investigate the lattice structure and temperature factors. Powder samples will be used, and the effects of particle size on the extinction of low angle Bragg reflections will be carefully examined.

II. BACKGROUND

A. TITANIUM-ALUMINUM ALLOYS

1. Development and Utilization

Titanium alloys have seen extensive utilization in a wide variety of technologies due to their exceptional resistance to oxidation and corrosion and high melting temperature. Applications in marine environments and medicine as well as chemical and petroleum engineering have taken advantage of these properties. Additional benefits of decreased density, high temperature strength and stiffness, and creep resistance have been gained with certain alloying elements, most notably aluminum. These characteristics attracted the aerospace industry to the further development of titanium aluminides. [Ref. 4]

Much of the emphasis in early research was placed on titanium rich Ti-Al alloys, in particular those containing less than 10 wt.% aluminum. These alloys were used in jet engine components subjected to low and mid-range temperatures [Ref. 1, p. 37]. Ti-6Al-4V (wt%) was developed in the 1950's and has seen the most widespread use in aerospace applications [Ref. 4, p. 106]. As aircraft engines developed more power with increased operating temperatures, advances in the conventional titanium alloys have kept abreast. Recently, however, limitations in operating temperatures have been reached for these alloys; currently the most significant of new materials such as IMI829 (Ti-5.5Al-3.5Sn-3Zr-1Nb-0.25Mo-0.25Si) show a decline in performance at temperatures above 550

to 580°C [Ref. 4, p. 106]. Future applications in both jet engine components and airframe structures will require alloys of more durable oxidation resistance and greater strength at still higher temperatures.

The ordered intermetallic compounds Ti_3Al and $TiAl$ show excellent potential for surmounting these problems. They exhibit considerable oxidation resistance and high strength at temperatures exceeding conventional alloys. With the additional and significant advantage of low density they are a natural alternative for aerospace applications, provided problems of ductility at low temperature are overcome.

2. Current Research Emphasis

The driving factor behind recent research into Ti_3Al and $TiAl$ is the problem of counteracting the inherent brittleness of these phases at temperatures below approximately 600°C. Various solutions have been proposed including both conventional and unconventional processing techniques and dispersion strengthening through alloying additions. Among the topics of study:

- Development of alloys through powder metallurgy methods of mechanical alloying. [Ref. 5], [Ref. 6]
- Dislocation and slip system analysis of deformation mechanisms. [Ref. 7], [Ref. 8]
- Phase transition characteristics and microstructural features. [Ref. 9], [Ref. 10]
- Rapid solidification processing methods. [Ref. 11]
- Alloying additions and dispersion strengthening effects. [Ref. 4], [Ref. 12]

Several studies have touched on the comparative benefits of these two binary compounds, with advantages and disadvantages attributed to both. While some increase in low temperature ductility over TiAl has been noted in Ti_3Al , the latter is more susceptible to oxidation and hydrogen permeation. In addition, TiAl has improved strength in part due to its single phase ordered structure which persists right up to its melting point of 1450°C. [Ref. 13]

B. MATERIAL CHARACTERISTICS

1. Microstructure

Up until 1951 information on the Ti-Al system was limited to the aluminum rich end of the phase diagram. It was not until the work of Ogden *et al.* that some of the features concerning the γ -TiAl phase and the solubility of aluminum in α titanium were identified [Ref. 14]. The current phase diagram is shown in Figure 1 [Ref. 15].

a. γ Phase

The γ -TiAl phase is an ordered intermetallic compound spanning a range of approximately 49 to 55 at.% aluminum at room temperature. It is classified as an $L1_0$ (AuCu) type alloy with a face centered tetragonal lattice structure.

Recent research has been conducted to clarify uncertainties in the high temperature fields of Ti_3Al [Ref. 16] and TiAl [Ref. 9]. The region of dispute for the γ phase was at temperatures above approximately 1000°C, specifically at a composition of Ti-50at.%Al. Murray has predicted the formation of β dendrites

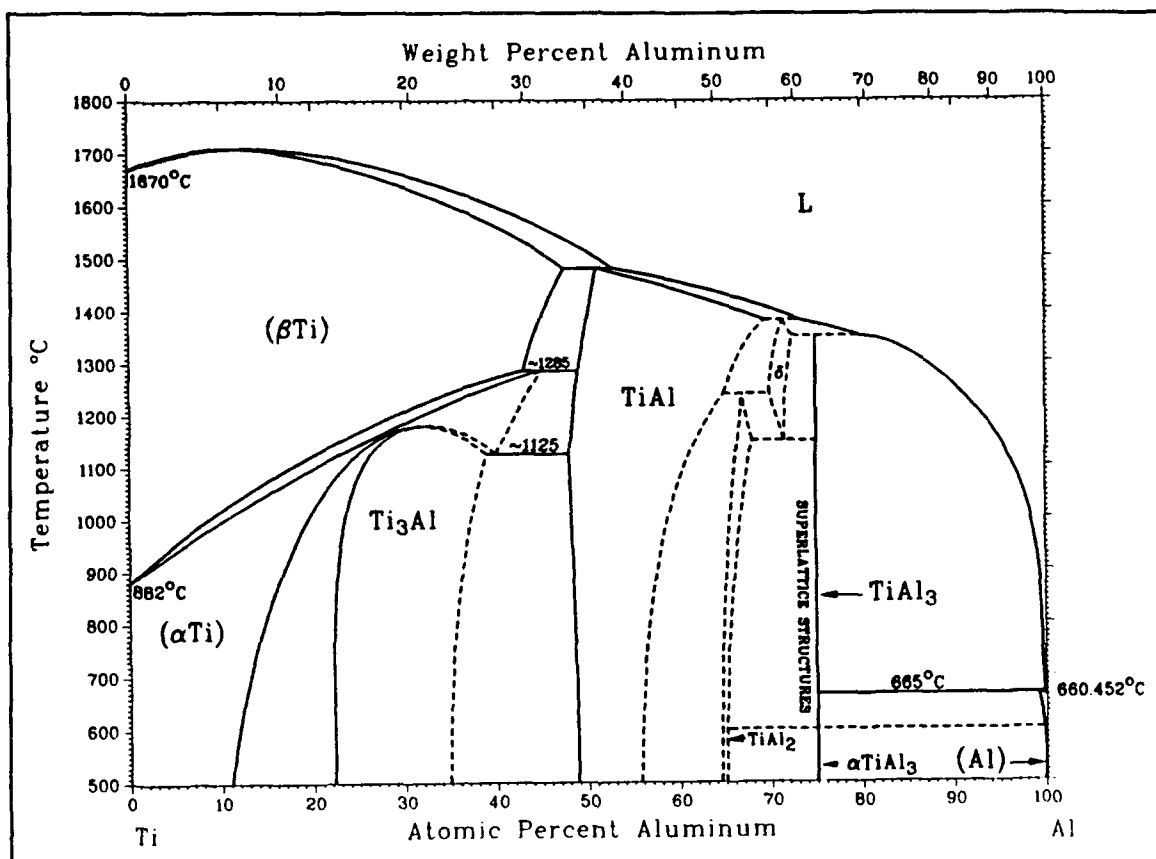


Figure 1. Ti-Al Phase Diagram

surrounded by γ due to the peritectic reaction $L + \beta \rightarrow \gamma$ [Ref. 17]. The β -phase then transforms to $(\alpha_2 + \gamma)$ at room temperature; α_2 is an ordered version of the α -phase. However, McCullough and others have found that hexagonal α dendrites form upon cooling from the liquid rather than the body-centered cubic β , and have suggested the inclusion of a high temperature α field in the phase diagram [Ref. 18]. The area under debate is shown in Figure 2 [Ref. 19, p. 1344]. The dotted lines correspond to the results obtained by McCullough *et al.* and are consistent with earlier phase diagrams of this system. The solid lines represent the current version researched by Murray.

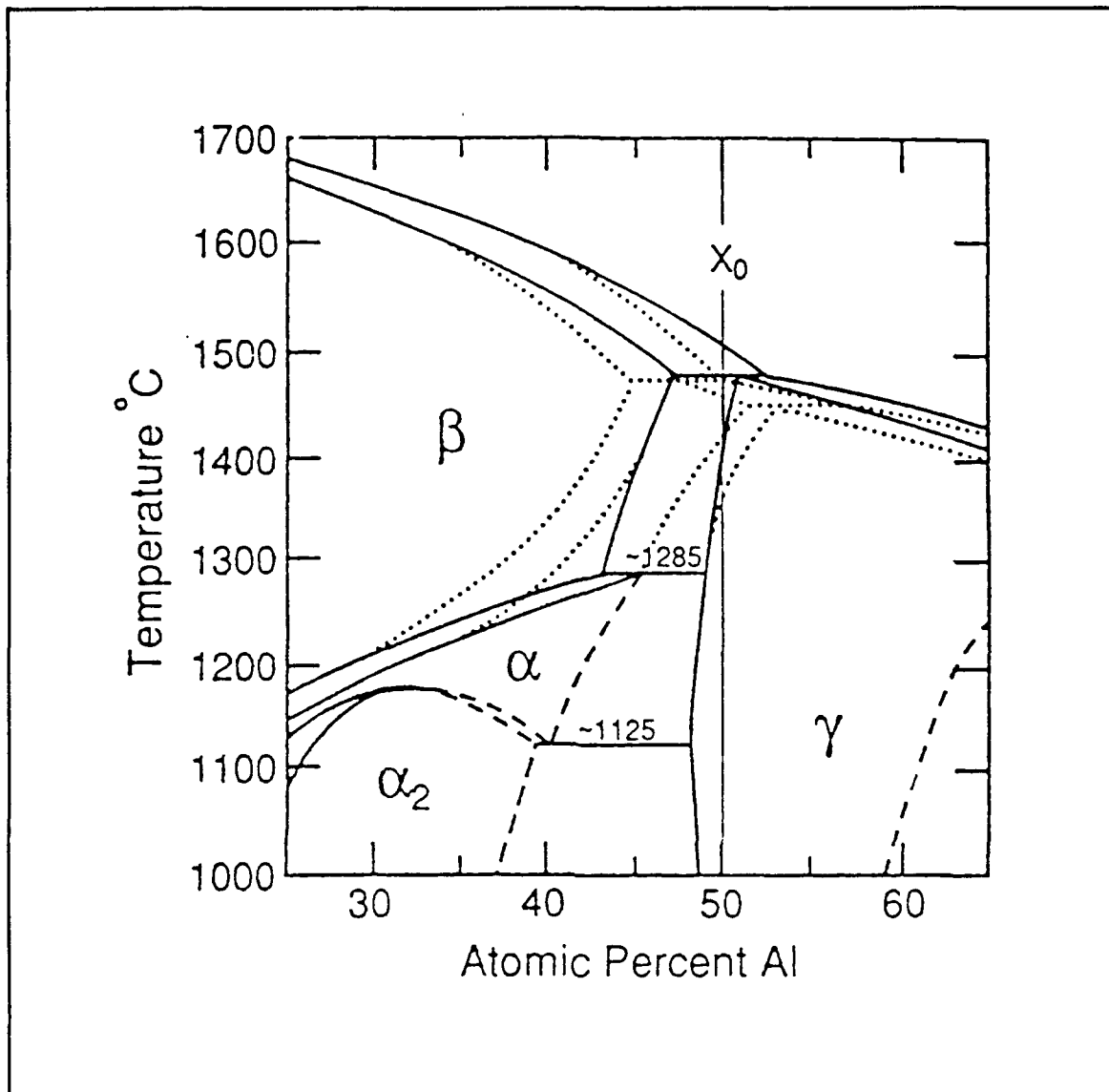
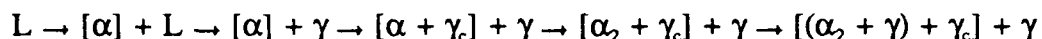


Figure 2. Proposed Alterations to the Ti-Al Phase Diagram

From their studies McCullough *et al.* have shown that with decreasing temperature the α dendrites undergo a decomposition which includes the formation of cellular γ_c in addition to the γ -segregate. The γ -segregate does not undergo any transformation and remains stable at all temperatures. The evolution of the solidification process includes a second peritectic reaction and can be summarized as:



This path is followed by alloys in the range of approximately 49-55 at.% Al. [Ref. 9, p. 1335]

b. Crystallography

The face-centered tetragonal $L1_0$ unit cell of γ -TiAl is shown in Figure 3. At the stoichiometric composition it has a c/a ratio of 1.02, and therefore its symmetry is essentially the same as a face-centered cubic lattice. Over a composition range from 46 to 62 at.% Al the tetragonality increases from 1.017 to 1.026. This is due to the substitution of aluminum atoms for titanium; since the atomic radii of Al and Ti are approximately 1.43 and 1.48 Å respectively, the contraction of the unit cell takes place only in the basal plane, thereby resulting in expansion in the c direction. It has been suggested that this expansion is due to an increase in electron concentration with the addition of aluminum. [Ref. 20]

The γ -phase remains ordered up to its melting point; this is a source of its high temperature strength and stiffness. While TiAl is based upon the AuCu structure, its ordering has different origins. In AuCu long range ordering is derived from a disordered face-centered cubic structure. In γ -TiAl the ordering takes place during the transformation from liquid to solid or through a peritectic reaction. Li *et al.* have also shown that long range ordering can be suppressed by rapid quenching from the melt [Ref. 21]. Their research indicated that antisite substitution was the leading defect mode in aluminum rich TiAl.

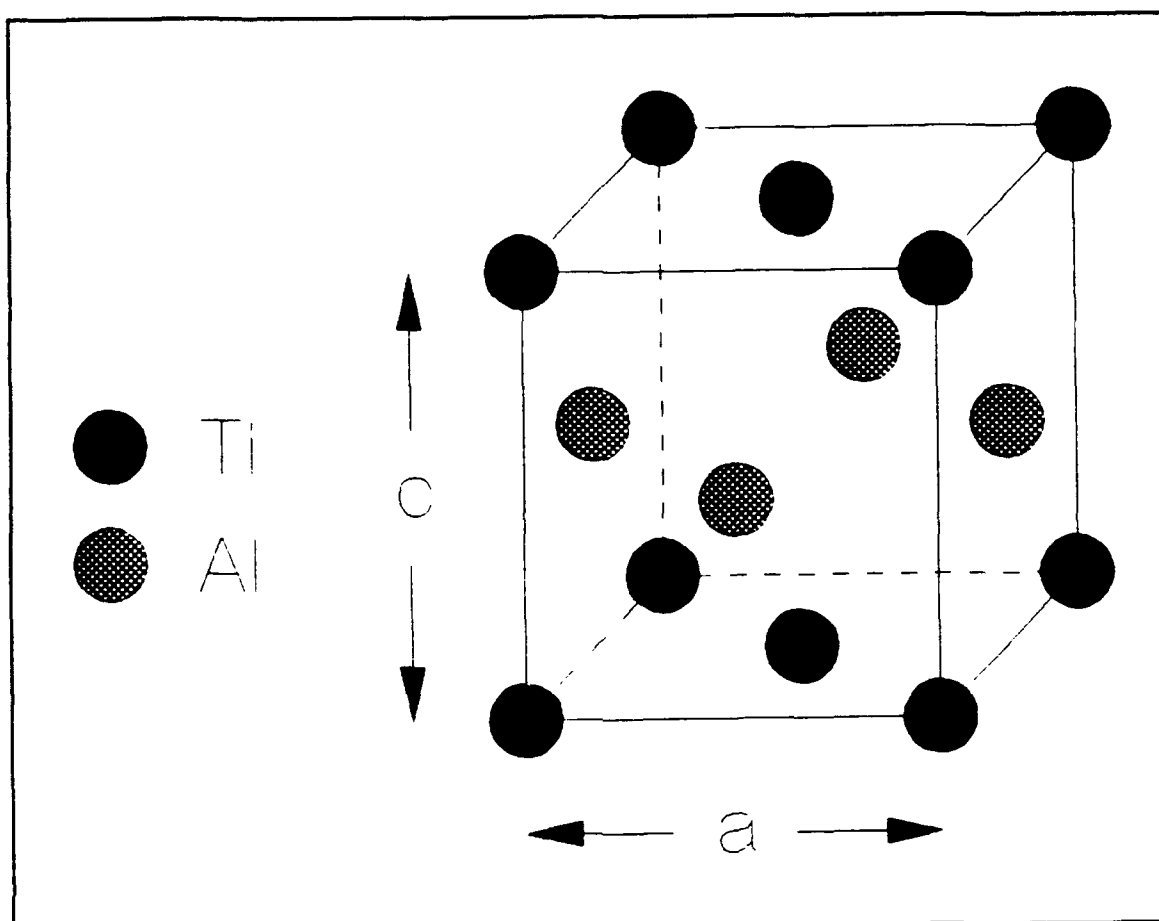


Figure 3. $L1_0$ Lattice Structure of γ -TiAl

2. Engineering Properties

A summary of the properties of conventional titanium alloys, nickel-based super alloys, Ti_3Al , and TiAl is given in Table 1 [Ref. 13, p. 353]. The advantages of TiAl over the other common high temperature alloys are clearly evident, as is the disadvantage of low room temperature ductility.

a. *Deformation Mechanisms and Ductility*

The most significant property of TiAl is its ductile to brittle transition behavior at approximately 700°C. Lipsitt *et al.* first identified this feature in 1974 by

Table 1. PROPERTIES OF HIGH TEMPERATURE ALLOYS

Property	Ti Base	Ti ₃ Al	TiAl	Superalloys
Density (g/cm ³)	4.5	4.15-4.7	3.76	8.3
Young's Modulus (GPa)	110-96	145-110	176	206
Max. Temp.--Creep (°C)	538	815	1038	1093
Max. Temp.--Oxidation (°C)	593	649	1038	1093
Ductility--Room Temp. (%)	~ 20	2-5	1-2	3-5
Ductility--Operating Temp. (%)	High	5-8	7-12	10-20

conducting tensile tests at various temperatures from 25 to 1000°C [Ref. 22]. Their research revealed the ordering of γ -TiAl throughout this temperature range and a rapid change in mechanical properties between 600 and 900°C. Through observations of dislocation activity by electron microscopy, they attributed the mechanical behavior of TiAl to the mobility of $1/6[112]$ partial dislocations, a component of the $[011]$ superdislocation. The $1/6[112]$ partial was found to be pinned at temperatures below 630° by an unknown source, while above 700°C it was mobile. This partial is also a twinning dislocation and consequently twinning becomes increasingly important above the transition temperature. The $L1_0$ structure with possible Burgers vectors identified is shown in Figure 4.

Lipsitt's work precipitated a large number of subsequent studies which were directed towards identifying the source of pinning and the relationship of twinning in the deformation process. The pinning of the $1/6[112]$ partial was suggested by Hug and coworkers to be a result of faulted dipoles caused by a complicated dislocation jog

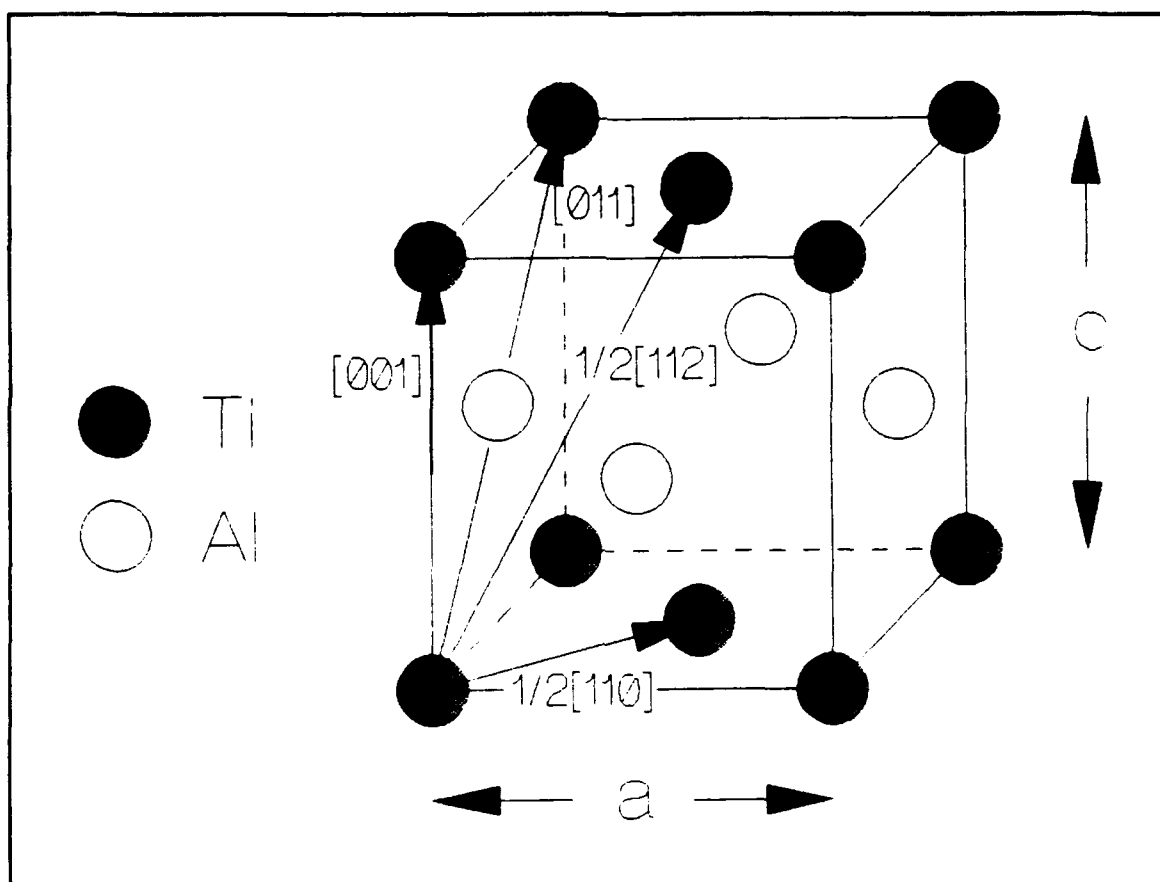


Figure 4. Possible Burgers Vectors in TiAl

mechanism [Ref. 8]. As the deformation of samples was increased larger numbers of these dipoles were observed, thereby increasing the restriction on dislocation motion and causing hardening of the material. This same group of researchers identified other dislocation systems active in TiAl and in a later paper established that dislocations with Burgers vector $b=1/2[110]$ are sessile at room temperature [Ref. 23]. Greenburg *et al.* suggested that the mobility of these dislocation systems is caused by electron charge density anisotropy near the Ti atoms in TiAl [Ref. 24]. The anisotropy causes the dislocations to be trapped in Peierls stress valleys, thereby reducing their mobility.

The results of research conducted by Court, Vasudevan, and Fraser verified that the anisotropy in charge density distribution is due to directional bonding among Ti atoms. This covalency contributes to the locking of the $1/2\langle 110 \rangle \{111\}$ ¹ slip systems and will be dependent on the composition and purity of the alloy. Court *et al.* concluded that thermal activation would effectively reduce the Peierls stress and hence allow increased dislocation mobility. This characteristic would explain the rise in ductility at higher temperatures. [Ref. 7, p. 157]

While Court *et al.* expected twinning dislocation mobility to increase with temperature thereby also contributing to improved ductility, they found no increase in twin density at elevated temperatures [Ref. 7, p. 156]. Other researchers have expanded upon the original identification of twinning in TiAl [Ref. 25] and its effects [Ref. 22]. Feng *et al.* have found additional twin orientations in studies of TiAl of various compositions and have confirmed their importance in the deformation of this compound [Ref. 26], [Ref. 27]. Hanamura and Tanino, among others, have investigated alloying addition affects on twinning [Ref. 28]. Additional research in this area is required to fully understand the role of twinning on ductility improvement.

b. Other Fracture and Embrittling Mechanisms

In addition to the extraordinary effect on ductility exhibited by dislocation activity and the associated covalency consequences of anisotropic electron charge density distribution, a number of other factors contribute to the mechanical behavior of TiAl.

¹The notation $\langle hkl \rangle$ refers to all permutations of $\pm h$ and $\pm k$ as established by Hug *et al.* [Ref. 23].

Much of the other research into engineering properties has been concerned with the impact of variation in alloy composition on fracture behavior.

Early investigations of the Ti-Al system by Bumps, Kessler, and Hansen in the 1950's first identified the embrittling consequences of increased aluminum content. Besides confirming a number of physical properties including melting point, lattice structure, and solubility limits, Bumps *et al.* established the hardening capabilities of aluminum over a wide range of compositions. Particularly interesting was the sharp decrease in Vickers hardness as aluminum content was increased into the γ single phase region, shown in Figure 5 for the as-cast alloy and indicated heat treatments. [Ref. 29]

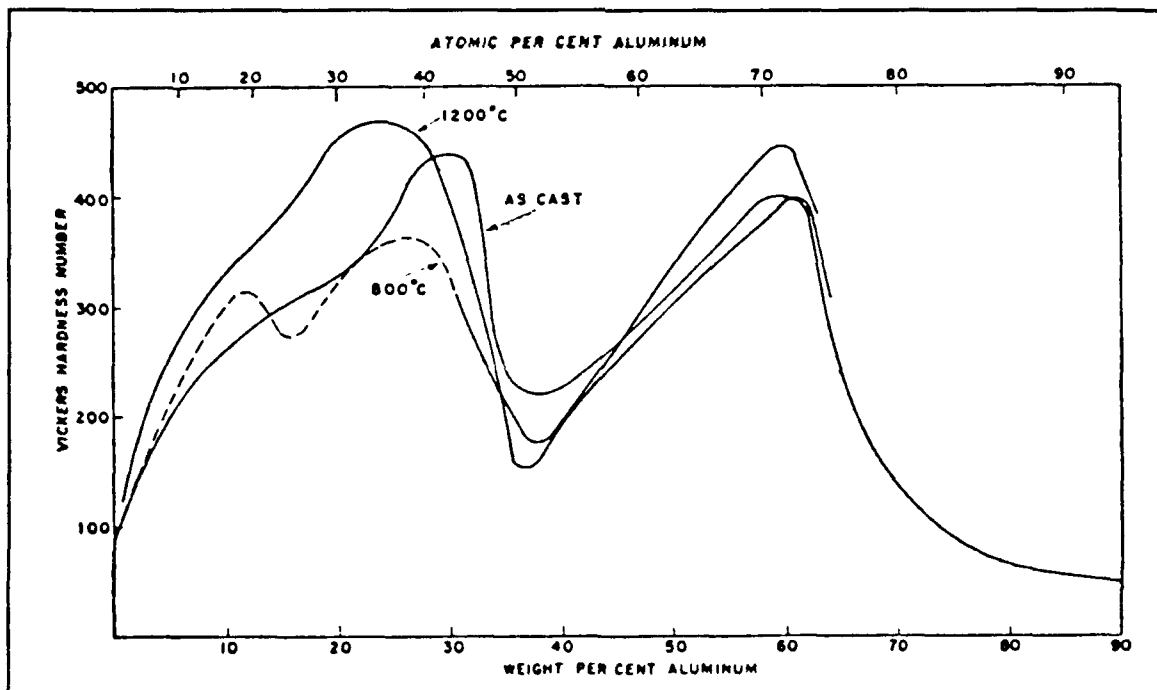


Figure 5. Vickers Hardness vs. Composition

A more recent and comprehensive study was undertaken by Huang and Hall concerning composition and microstructure effects on deformation behavior. These researchers considered alloys with aluminum concentrations from 46 to 60 at.% Al, resulting in the following conclusions: [Ref. 30, p. 438]

- Microstructure has a strong effect on mechanical properties. The ($\gamma + \alpha$) duplex structure is more readily deformed than single phase γ -TiAl.
- Mechanical properties are dependent upon composition; only alloys of compositions from 48 to 54 at. % Al show any appreciable plasticity. Within this range a transition occurs at approximately 51 at.% Al; the low-Al alloys exhibit twice as much plasticity as the high-Al alloys. This transition corresponds to a change in microstructure from duplex to single phase, based on the previously mentioned revised phase diagram suggestions of McCullough *et al.* [Ref. 9] and shown in Figure 6.
- Differences in dislocation behavior between the low- and high-Al regions noted above were found. $1/2[110]$ dislocations were observed in both regions, but the deformation of the duplex alloys is also facilitated by $\{111\}$ twinning; slip of $[101]$ and $1/2[112]$ superdislocations contribute to additional deformation of the single phase alloys.
- The alloy with composition Ti-52at.%Al showed changes in deformation modes from single phase to that of duplex phase at 260°C. There is no further change at the ductile-to-brittle transition temperature.
- Fracture of γ -base alloys occurs by a mix of cleavage and grain boundary failure. At liquid nitrogen and room temperatures cleavage is the dominant mode while at temperatures near the DBTT intergranular failure dominates.

Examination of grain size and boundary characteristics has also been undertaken for additional information concerning embrittling mechanisms. Most of this research has been concerned with the interaction of grain boundaries in the $\alpha_2 + \gamma$ two phase region. A discontinuous coarsening reaction involving grain boundary migration of lamellar structures was observed by Shong and Kim at composition 43 at.% Al which

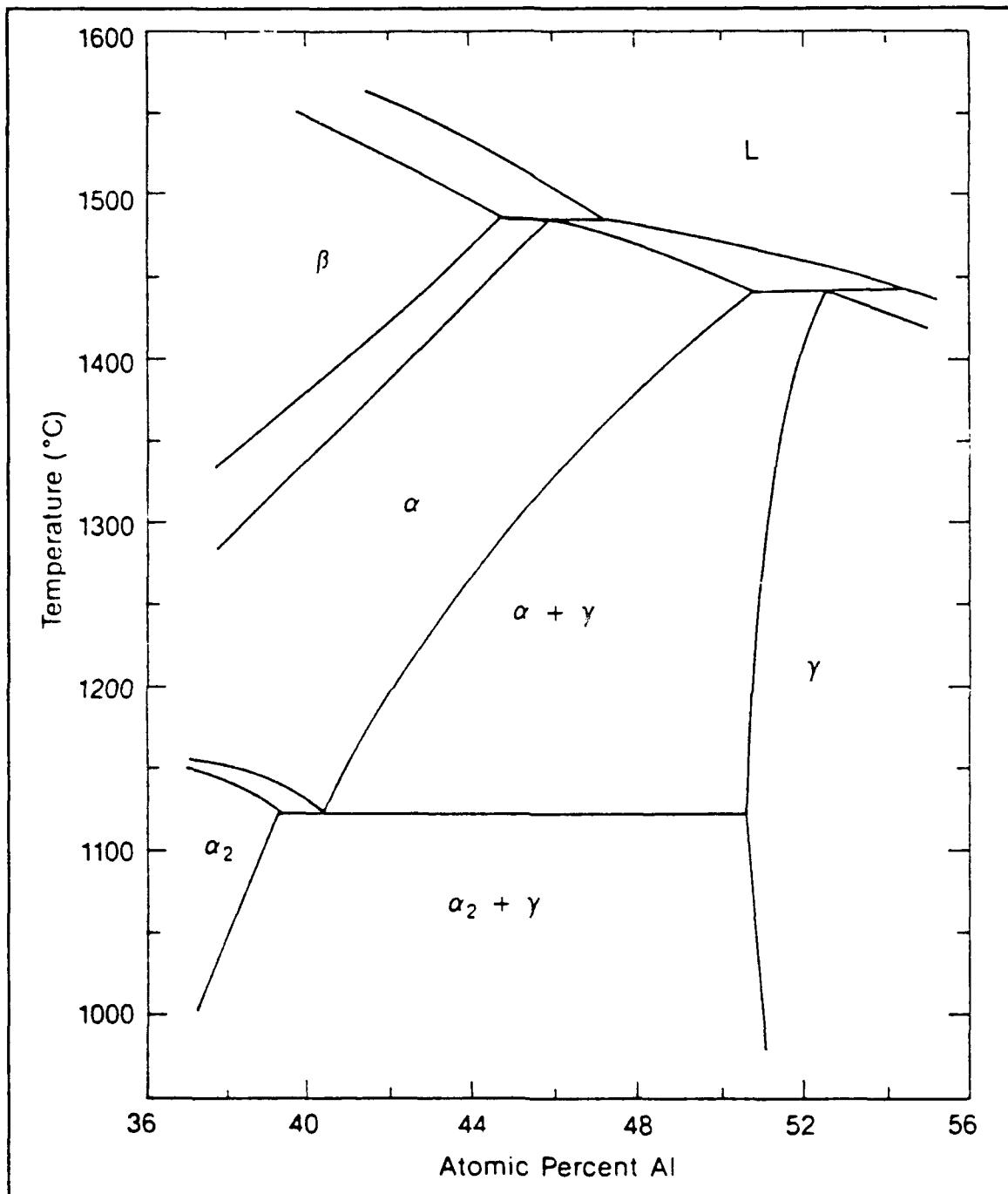


Figure 6. Partial Ti-Al Phase Diagram (Proposed) [Ref. 30, p. 428]

no doubt contributes to the deformation mode in this region [Ref. 31]. Gertsman *et al.* conducted a study of grain boundary geometry of Ti-52at.%Al and proposed that boundary misorientation may be an additional cause of poor ductility [Ref. 32]. An investigation of the effects of grain boundary orientation on twinning by Schwartz and Sastry pointed to still another deformation mechanism operating in γ - and ($\alpha_2 + \gamma$)-TiAl [Ref. 33].

c. Impurities and Alloy Addition Effects

The addition of other elements to the Ti-Al system is an obvious method of altering the engineering properties. Various ternary additions have been investigated, with encouraging results in ductility improvement. The motivation behind this research was earlier successes with other intermetallics, most notably in the Ni-Al system.

A large part of the research in this area has been devoted to determining how the ternary atoms interrupt the ordering of TiAl, for this is a decisive factor in its high temperature strength. Konitzer *et al.* investigated the effects of niobium on Ti_3Al and TiAl and found through TEM studies that the Nb atoms preferentially occupy the Ti lattice sites in both alloy compositions [Ref. 12]. They suggested that this feature may increase the ordering energy of the alloy, with possible effects on ductility as a consequence. Niobium has also been found to affect the solidification and ordering path in the evolution of the γ -TiAl microstructure [Ref. 34].

Lattice site locations were also determined for gallium in TiAl by Ren, Chen, and Oliver; Ga was found to occupy the Al sites in TiAl, as expected due to its close proximity to Al on the periodic chart and the striking similarities in the lattice

structures of TiGa and TiAl [Ref. 35]. This research was spurred by Kad and Oliver's findings of reduced hardness in TiAl upon the introduction of Ga [Ref. 36].

Dislocation behavior is subject to alterations upon the introduction of ternary alloys. Hanamura and Tanino observed that samples of TiAl-2wt.%Mn exhibited improved ductility and attributed this to a twin boundary dislocation interaction which allowed the formation of glissile dislocations [Ref. 28, pp. 25-26]. Their research also provided evidence of room temperature dislocation behavior in Mn-added TiAl matching that of TiAl at high temperatures above the DBTT. Hug and Veyssi re achieved comparable results with a manganese-doped γ -TiAl and concluded that the sharp ductile to brittle transition may be attributed to a dislocation process assisted by diffusion [Ref. 37]. Similarly, tantalum has been shown to promote twinning and reduce the dislocation stacking fault energy, thereby increasing the number of glissile dislocations and improving ductility [Ref. 38].

The effects of boron on microstructure and dislocation activity in the two-phase ($\alpha_2 + \gamma$) region has been studied by Feng *et al.*, showing remarkable effects on high temperature phase development. Both boron and oxygen were found to enlarge the two-phase field, and boron permitted the retention of an ($\alpha_2 + \gamma$) lamellar structure upon quenching; contributions to high temperature stiffness by boron may be a resultant benefit. Boron was also found to reduce the c/a ratio of the face-centered tetragonal $L1_0$ structure by occupying the octahedral interstitial sites (see Figure 7) and producing a local distortion which is larger in the a -direction than in the c -direction. For the normal c/a

ratio of 1.02 in TiAl only one set of misfit dislocation arrays are possible, but with the composite addition of boron the reduction in c/a allows three misfit dislocation arrays due to the face-centered cubic character of such a structure. This feature would facilitate an increase in plastic deformation capability. [Ref. 39], [Ref. 40]

The exposed surfaces of TiAl are similar to ceramic surfaces in that they are prone to microcracks which would clearly affect the mechanical behavior of the material. Saito and Matsushima investigated methods to improve surface properties by implanting nitrogen ions into TiAl specimens of composition 34, 36, and 38 wt.% Al. Nitrogen ions were selected due to their predictable occupation of interstitial lattice sites,

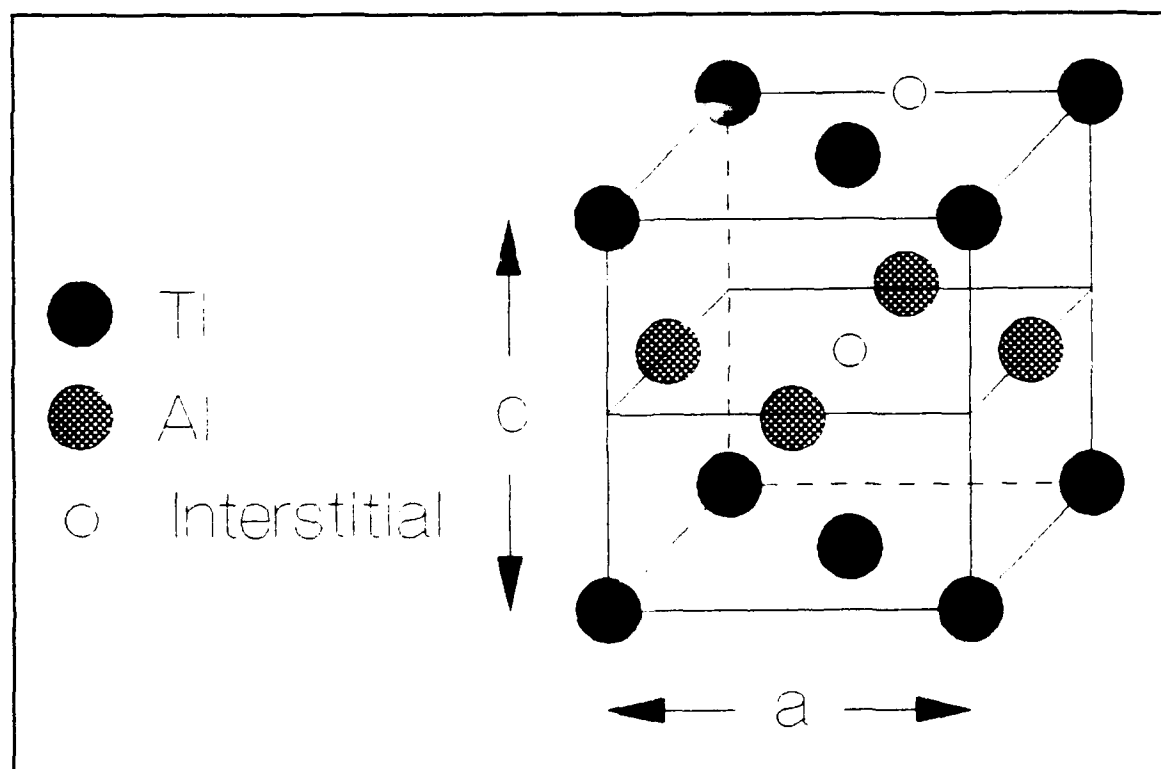


Figure 7. The Octahedral Interstitial Site in TiAl

nitride formation effects, and inducement of disordering of the ordered TiAl structure by radiation damage. Their results yielded several observations: [Ref. 41]

- Surface hardness increased dramatically by ion implantation, reaching as much as three times that of the unimplanted specimen for certain ion doses. There was a change in hardness across the composition range, with values at stoichiometric TiAl being the lowest and rising significantly on both sides of this midpoint. This was attributed to vacancy defects caused by ion radiation damage. Dispersion hardening by the formation of nitrides and solid solution hardening due to solute nitrogen were also cited as reasons for increased hardness.
- Ion implantation caused complete removal of surface microcracks. This was theorized to be a result of residual compressive stresses induced by excess solute nitrogen and to nitrides resistant to corrosion present in the implanted surface layer.
- Fracture tests showed changes in fracture modes from intergranular to transgranular following implantation, suggesting that embrittlement due to grain boundary effects may be reduced by this method.

3. Methods of Analysis

Because of the covalent vice metallic nature of bonding in titanium aluminides, it is critical to an understanding of the bonding mechanisms that the distribution of valence electrons be investigated. The benefit is more complete information on the directionality of bonding and concentration of electrons surrounding the interstitial sites. This subsequently would help explain the changes in physical properties brought about by alloying additions and the difficulty in promoting full slip system operation at low temperatures.

Theoretical predictions of electron charge densities have been completed by Hong *et al.* for Ti_3Al based on a complicated method of numerical and linear wave function analysis [Ref. 42]. Their resulting charge density map for the (0001) plane of the D0_{19} hexagonal structure is shown in Figure 8 and is an excellent example

of the useful information to be gained from such a representation of electron distribution. The values of electron density are noted with charge buildups identifying the covalent attraction between atoms. Positions I, II, and III are interstitial sites of local contour minima or maxima; from a knowledge of corresponding atom positions in neighboring planes Hong *et al.* theorized that bonding between Ti and Al is weak while the aluminum atoms promote strong bonding between like Ti atoms [Ref. 42, p. 1947].

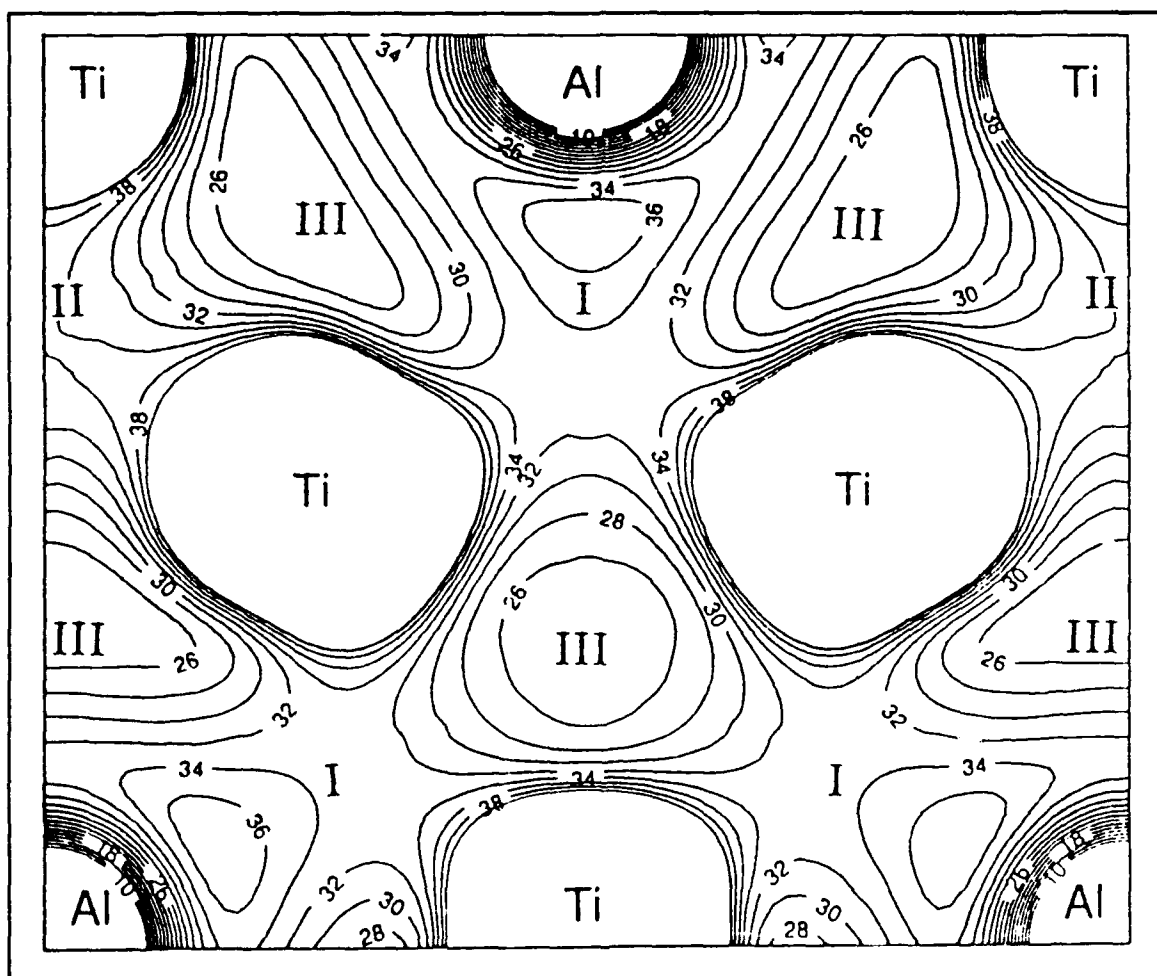


Figure 8. Charge Density Contours of the D0₁₉ (0001) Plane

In order to discern detailed information concerning bonding characteristics a comparison must be made between experimental and theoretical charge density distributions. To acquire the experimental distribution a Fourier sum is employed:

$$\rho(x,y,z) = \frac{1}{\Omega} \sum_h \sum_k \sum_l F_{hkl} \exp[2\pi i(hx + ky + lz)] \quad (1)$$

where $\rho(x,y,z)$ is the electron density at the point (x,y,z) in a unit cell of volume Ω , F_{hkl} is the atomic structure factor, and h, k, l the Miller indices [Ref. 3, p.671]. Electron charge density distributions are therefore highly dependent on accurate measurement of atomic structure factors. A number of methods are available to accomplish this, including X-ray Pendellösung measurements, γ -, X-ray, and electron diffraction; a short summary of each follows.

a. X-ray Pendellösung Measurement

This method uses an X-ray diffractometer with a single crystal specimen to measure the spacing of diffraction phenomena known as Pendellösung fringes. These fringes are generated by the change in extinction distance observed with different X-ray wavelengths. Extinction distance refers to the period of oscillation of two interfering waves which are propagated in the transmitted and diffracted directions when the sample is irradiated with X-rays. The extinction distance can be expressed as a function of the structure factor; hence structure factors can be measured by either making a topographic record of fringe spacing or by using solid state X-ray detection devices to examine the fringe spacing at different angles of diffraction. Accuracies in structure factor

measurement as good as $\pm 0.1\%$ have been observed using this method, though this is highly dependent on the quality of the single crystal used. [Ref. 43]

b. γ -ray Diffraction

Very similar to conventional X-ray diffraction, this method instead uses γ -rays as the diffracted energy source. Its advantages lie in its reduced absorption due to wavelengths which are shorter than X-radiation. Because of this, corrections for extinction and dispersion scattering are minimized, thereby reducing the errors in measurement of structure factors. Accuracies of up to $\pm 0.2\%$ have been recorded using this method. [Ref. 3, p. 673]

c. Electron Diffraction

There are several methods of analysis available using the transmission electron microscope (TEM), the most accurate of which is the critical voltage method. Fox and Tabbernor have obtained excellent results by this technique in measurement of structure factors for β' -NiAl [Ref. 3]. It involves the identification of a critical electron accelerating voltage which corresponds to a very small diffracted beam intensity at second order or higher reflections, resulting from destructive interference. The critical voltage is sensitive to the chemical potential of the crystal, and from this dependence structure factors with a high degree of accuracy can be determined [Ref. 44]. The disadvantage in this method is its limitation to low angle Bragg reflections. Its advantage is that sample preparation is less complicated than for X-ray diffraction and very small volumes of material can be analyzed [Ref. 45].

d. X-ray Diffraction

The most general and well established method of analysis uses X-radiation of samples to determine structure factors. X-ray diffraction (XRD) provides information on both fundamental and superlattice reflections across the entire spectrum of possible Bragg angles. In addition to diffracted intensity measurements required for structure factor analysis, XRD allows for accurate determination of lattice parameters based on reflection peak positions. Powder X-ray diffraction is particularly suitable in that it eliminates the need for a single crystal of extremely high quality and avoids several side effects associated with diffraction of a solid specimen. Results from previous studies on β' -NiAl alloys by Cooper [Ref. 2] and Hughes *et al.* [Ref. 46] have shown this method to be quite viable in determination of Debye-Waller temperature factors. For these reasons this technique was selected for use in the present study.

C. FUNDAMENTALS OF X-RAY DIFFRACTION

1. X-Ray Diffraction Geometry

The diffraction of X-ray energy is dependent on Bragg's Law:

$$n\lambda = 2d\sin\theta \quad (2)$$

λ is the wavelength of incident X-radiation, d is the interplanar spacing of the crystal structure, and θ is the angle of reflection. The diffraction geometry is shown in Figure 9 [Ref. 47, p. 131]. The advancing wave front AA' strikes the regularly spaced planes p_n and the diffracted energy is measured at the detector D . The detector

moves through an angle of 2θ while the sample moves through an angle θ . For a face-centered tetragonal lattice structure, as is the case with TiAl, the distance between planes of Miller indices (hkl) is given by Equation (3),

$$\frac{1}{d} = \sqrt{\frac{h^2 + k^2}{a_0^2} + \frac{l^2}{c_0^2}} \quad (3)$$

where a_0 and c_0 are the lattice parameters.

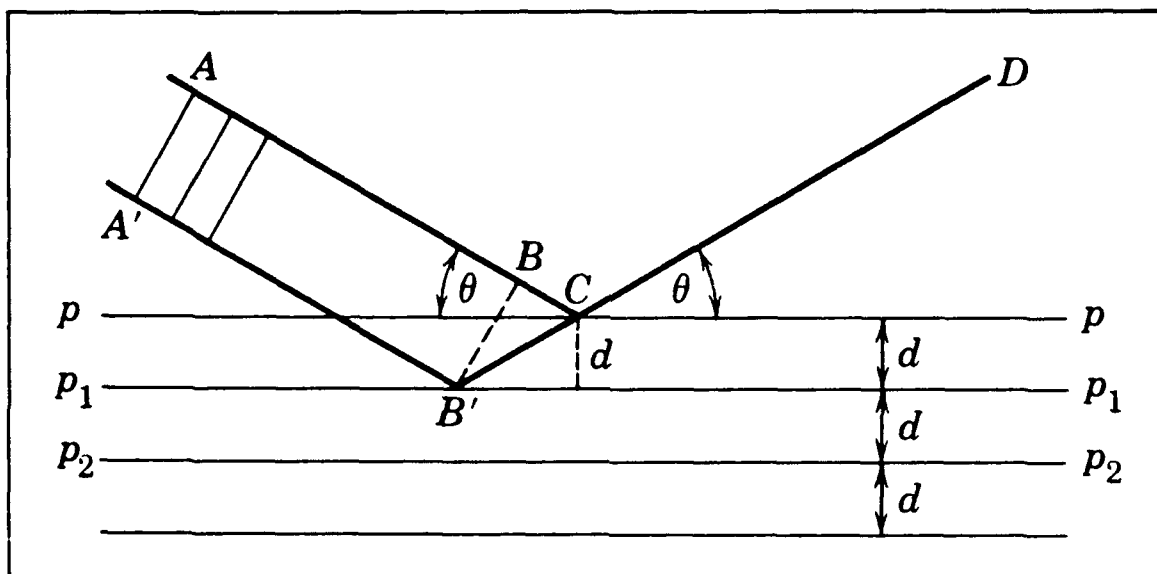


Figure 9. Bragg's Law Geometry

Upon reflection the diffracted energy is detected and processed, with the usual result a plot of intensity as a function of 2θ , as shown in Figure 10 [Ref. 47, p. 284]. This particular peak clearly shows a $K\alpha_2$ doublet as a result of two separate wavelength components of the incident radiation. The wavelengths are only slightly different from one another and hence there is some overlapping of reflection from each component as a result. The area under the peak represents the total diffracted intensity; relative

intensities for each peak are determined by measuring the total area and subtracting out the background radiation indicated by levels on either side of each peak. The experimental relative intensity values are used to calculate the Debye-Waller temperature factor in a method to be presented later.

2. Factors Affecting Diffracted Intensities

Several factors figure into the intensity levels observed by the detection device. For powder diffractometry, the intensity generated by each set of reflecting planes can be represented as:

$$I = K / F^2 p \phi(\theta) \exp^{-2M} \quad (4)$$

K is a constant of proportionality dependent on the diffractometer and other laboratory equipment characteristics, F is the atomic structure factor, p is the multiplicity factor, $\phi(\theta)$ is the Lorentz-Polarization correction, and M is the temperature factor. Each of these factors and additional influences on diffracted intensities will be discussed briefly.

a. Atomic Structure Factor

Since the lattice structure of a crystal is dependent upon the regular repetition of atoms within a unit cell, the energy diffracted by the structure as a whole is subject to the amount reflected by each individual atom. The structure factor is hence a measure of the amplitude of the wave diffracted by the unit cell relative to its constituent atoms. By varying the Bragg angle, the repetitive nature of the lattice allows for different planes of atoms to become involved in the diffraction of energy. By

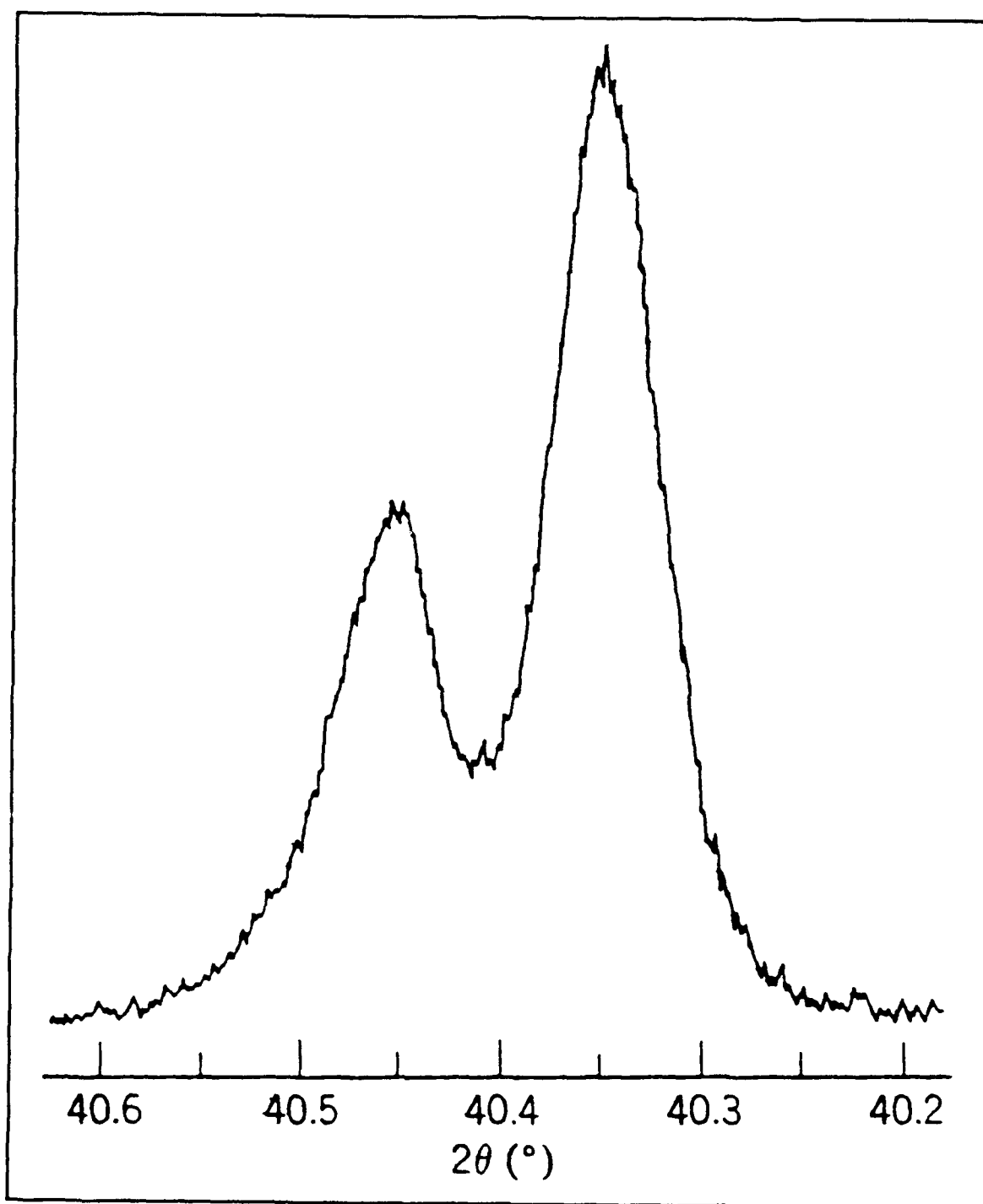


Figure 10. Intensity Peak with $K\alpha_2$ Doublet

combining the observation of diffracted intensity with each planar spacing satisfying Bragg's law, the location of individual atoms within the lattice structure can be deduced.

In order to determine the structure factor F , the amount of energy reflected from each atomic point source within the lattice must be accounted for. Thus, the structure factor can be expressed as a sum of the diffraction contribution of each n th atom at position uvw of the unit cell containing N total atoms, given by Equation (5) as

$$F_{hkl} = \sum_N f_n \exp[2\pi i(hu_n + kv_n + lw_n)] \quad (5)$$

where f_n is the atomic scattering factor. Thus for off-stoichiometric TiAl of composition m at.% with Ti atoms assumed at positions $uvw = 000$ and $\frac{1}{2}\frac{1}{2}0$ and Al atoms at $0\frac{1}{2}\frac{1}{2}$ and $\frac{1}{2}0\frac{1}{2}$, Equation (5) reduces to

$$F_F = 4(m_{Ti} f_{Ti} + m_{Al} f_{Al}) \quad (6)$$

for fundamental reflections (hkl all odd or all even) and

$$F_S = 4m_{Ti}(f_{Ti} - f_{Al}) \quad (7)$$

for superlattice reflections (hkl mixed).

b. Atomic Scattering and Dispersion

The atomic scattering factor is defined as the ratio of the amplitude of a wave scattered by an atom to the amplitude scattered by an individual electron, and is denoted by f_θ . Its value is equal to the atomic number Z at θ equal to zero and decreases with increasing values of θ for a given wavelength of radiation. The spatial distributions of electrons within a given atom are thereby accounted for under the assumption that the

electrons are essentially free electrons, with negligible binding energy compared to the energy of the scattered X-ray photon. In the case of an atom with an absorption edge close to the wavelength of the incident radiation, this is no longer true and an anomalous dispersion correction must be applied to the scattering factor. The total scattering factor is then represented as a complex number:

$$f = f_0 + \Delta f' + i\Delta f'' \quad (8)$$

where $\Delta f'$ and $\Delta f''$ are real and imaginary dispersion corrections, respectively. Values of f_0 , $\Delta f'$, and $\Delta f''$ are tabulated in the *International Tables for X-Ray Crystallography* for each of the elements, based on wavelengths commonly used in XRD [Ref. 48]. An analytical expression for calculating scattering factors is also noted in this work.

c. Multiplicity

The incident radiation beam may be reflected from several different planes, thereby increasing the diffracted intensity. The multiplicity factor p accounts for the proportion of planes which contribute to the same reflection and is equal to the number of planes of a form $\{hkl\}$ which possess the same interplanar spacing.

d. Lorentz-Polarization Factor

This is a combined factor which is dependent on the angle of diffraction. The Lorentz factor accounts for the variations in intensity across the interval surrounding the exact Bragg angle, which is due to the divergence and non-monochromatic nature of

the radiation beam. The polarization of the X-radiation is considered in the second part of the combined factor. The Lorentz-Polarization factor as a function of θ is:

$$\phi(\theta) = \frac{1 + \cos^2 2\theta}{\sin^2 \theta \cos \theta} \quad (9)$$

e. Temperature Factor

When considering the effects of the atomic scattering factor, it was assumed that the atom was at rest at a fixed lattice point. However, due to thermal vibration this ideal representation is inadequate for the determination of accurate structure factors. As the temperature is increased above absolute zero, the consequent increase in thermal vibration has three main effects [Ref. 49, p. 135]:

- An expansion of the unit cell occurs, causing changes in the interplanar spacing d and therefore in the 2θ positions of the diffraction peaks.
- The intensities of the diffraction peaks are decreased.
- The intensity of the background diffracted radiation is increased.

Thermal vibration causes imperfect diffraction to occur due to the mean displacement of atoms from the idealized lattice points. It has a greater effect on high angle reflections since the value of d is lower for these reflections. Consequently, for a constant X-ray wavelength values of intensity are decreased with increasing Bragg angle, as shown in Figure 11 for the example of iron at 20°C.

The calculation of the temperature factor is therefore dependent on a measure of thermal vibration and on the scattering angle, and can be represented as:

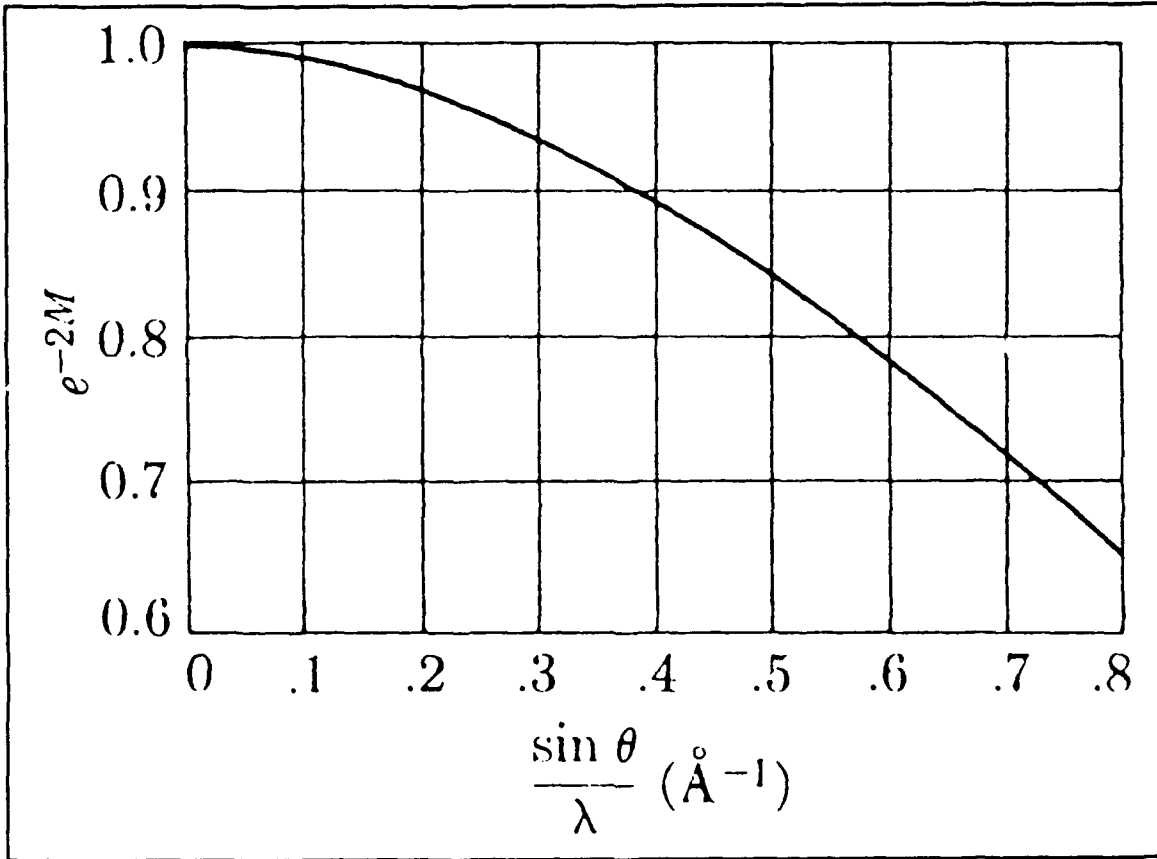


Figure 11. Temperature Factor of Iron at 20°C [Ref. 49, p. 136]

$$M = B \frac{\sin^2 \theta}{\lambda^2} \quad (10)$$

B is the Debye-Waller factor which is dependent on temperature and is extremely difficult to calculate accurately. Debye proposed the following expression for B [Ref. 47, p. 145]:

$$B = \frac{6h^2}{m_a k \Theta} \left[\frac{\phi(x)}{x} + \frac{1}{4} \right] \quad (11)$$

where h is Planck's constant, m_a is the mass of the atom, k is Boltzmann's constant, and $x = \Theta/T$, where Θ is the Debye characteristic temperature of the crystal expressed in degrees absolute. The Debye function $\phi(x)$ is given by the expression:

$$\phi(x) = \frac{1}{x} \int_0^x \frac{\xi d\xi}{e^\xi - 1} \quad (12)$$

This function and values of Θ are tabulated in the *International Tables* [Ref. 50], [Ref. 51].

f. Extinction

The incident beam of radiation which strikes a specimen has a small amount of its initial energy absorbed by the crystal structure. This effect will cause a continued decrease in diffracted intensity as the beam passes through successive planes. Reductions in intensity will also occur as a portion of the reflected beam is absorbed or reflected away from the detector by planes above it. If the crystal was ideally perfect, the eventual result would be total absorption of the X-ray and no observation of any diffracted intensity. For the ideally imperfect crystal, one in which crystal fragments are so small that negligible absorption takes place, the effective result would be diffraction of the full amount of incident energy. Of course these are the two extremes, between which exist actual specimen conditions. The reduction in diffracted intensity due to crystallite size of real imperfect crystals is known as extinction and its effect for various values of linear absorption coefficient μ is shown in Figure 12.

Since accurate structure factor determination is dependent on measured intensities of diffraction, extinction can have a dramatic effect on results and must be avoided if at all possible. For powder X-ray diffraction, the most obvious method of reducing the effects of extinction is to ensure that powder particles are as small as

possible. Only for particle sizes below approximately five microns can extinction be neglected.

g. Preferred Orientation

Upon deformation the crystal structure of a material may exhibit a preferred orientation, which can be a cause for decreased intensities in diffracted energy. Powder X-ray diffractometry promotes a random distribution of crystallite reflecting directions, thereby reducing the effects of preferred orientation.

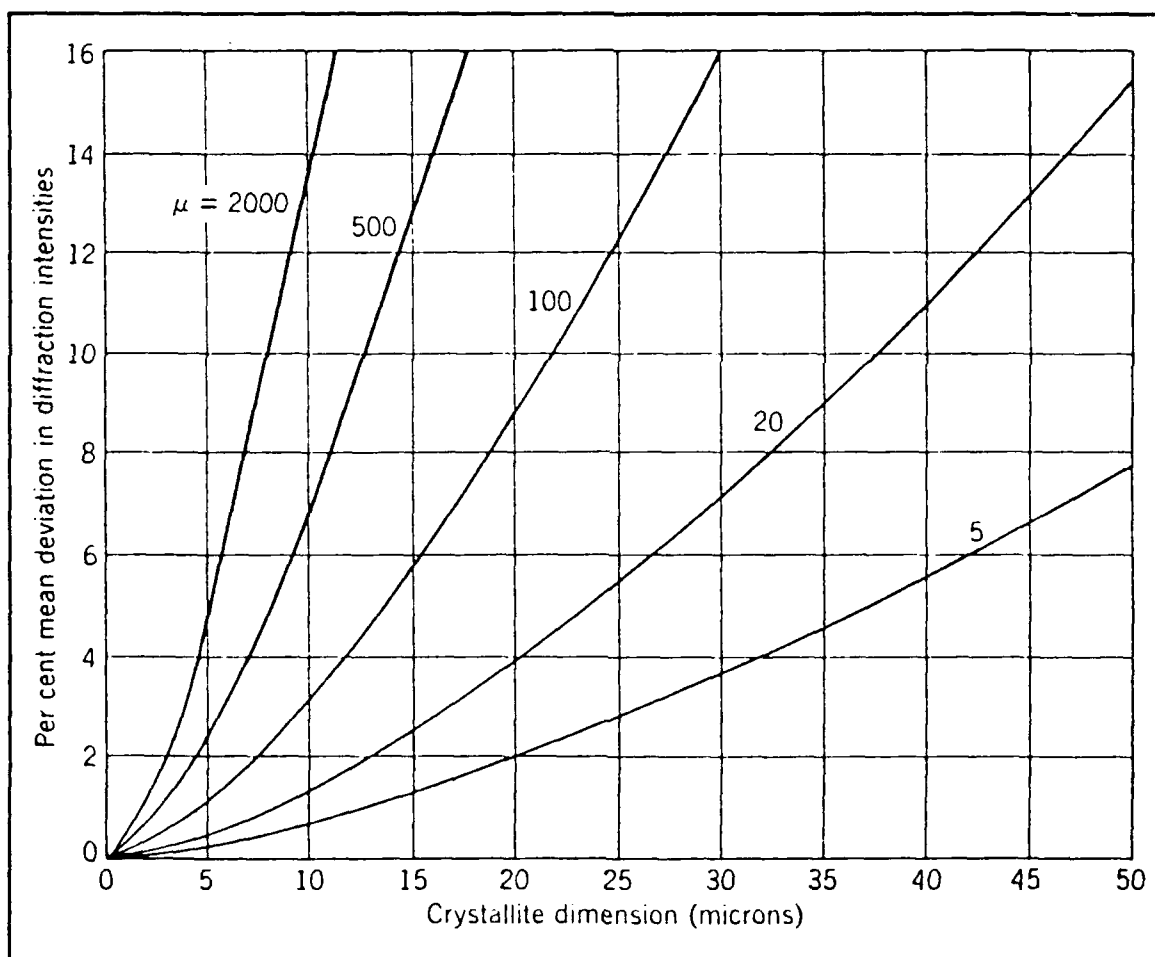


Figure 12. Intensity Deviation Due to Crystallite Size [Ref. 47, p. 367]

3. Lattice Parameter Determination

There are several methods of analysis available for the calculation of precise lattice parameters. This study will use a double extrapolation of values for c and a based on the Nelson-Riley function:

$$\frac{\Delta d}{d} = K \left(\frac{\cos^2 \theta}{\sin \theta} + \frac{\cos^2 \theta}{\theta} \right) \quad (13)$$

where K is a constant. Substituting in values of d and θ for $hk0$ and $00l$ peaks and extrapolating a least squares fit back to $\theta = 90^\circ$ will provide values of a_0 and c_0 respectively.

4. Debye-Waller Factor by the Wilson Method

Due to the difficulty in calculating theoretical values of the temperature factor, experimental Debye-Waller values are often used to determine structure factors. If we let

$$I' = \frac{I_{exp}}{p \phi(\theta) / F^2} \quad (14)$$

where I_{exp} is the experimental value of diffracted intensity, then

$$I' = K \exp \left(-2B \frac{\sin^2 \theta}{\lambda^2} \right) \quad (15)$$

Taking the natural logarithm of Equation (15), the resultant expression is:

$$\ln I' = \ln K - 2B \left(\frac{\sin^2 \theta}{\lambda^2} \right) \quad (16)$$

The values of $\ln I'$ are then plotted versus $\sin^2 \theta / \lambda^2$ for each diffraction peak and a least squares fit of the data is made. The resultant slope is equal to $-2B$ and the intercept is $\ln K$. Care must be taken when using this method to include only data points in which extinction is not a significant factor.

D. SCOPE OF PRESENT WORK

Several studies concerning electron charge density distribution, structure factor measurement, and determination of Debye-Waller values have been completed on other intermetallics, most notably NiAl. To the author's knowledge no such work has been completed on TiAl. In addition, published data on lattice parameters of alloys close to the composition under consideration in this study was last transcribed by Duwez and Taylor in 1952, using a Debye-Scherrer camera [Ref. 20]. The present research will investigate the lattice structure characteristics of the ordered intermetallic Ti-51at.%Al, to include:

- Accurate structure factor measurement using powder X-ray diffraction procedures and assessment of intensities by diffractometer methods.
- Determination of Debye-Waller temperature factors with comparison to melting point data and characteristic temperature.
- Examination of the effects of extinction due to powder particle size.
- Verification of the previous work by Duwez and Taylor concerning lattice parameter determination.

III. EXPERIMENTAL PROCEDURE

A. SAMPLE PREPARATION

An as cast, Ti-51at.%Al binary alloy was obtained from Wright-Patterson Air Force Base Materials Research Laboratory. Initial specimen analysis by the source indicated an oxygen content of approximately 700 ppm by weight.

In order to ensure the alloy was indeed single phase γ -TiAl the sample was homogenized at 1200°C and furnace cooled. It was then sealed in a silica tube, back-filled with argon, reheated to 1200°C, and water quenched to room temperature. Prior to the production of powder samples the surface oxide layer was removed by grinding using 240 grit silicon carbide paper.

The traditional method of filing to reduce the ingot to powder suitable for X-ray diffraction was found to be unacceptable in this case due to the extreme hardness of the alloy. Instead lathe turnings using a carbide-tipped blade were taken from the sample. The elongated turnings were then pulverized to a fine powder using a ceramic mortar and pestle. To relieve the consequent induced stress the powder particles were annealed at 900°C for 45 minutes; this was done in helium to avoid atmospheric contamination. Annealing time and temperature were chosen to circumvent any loss of aluminum content during the heat treatment.

B. MICROSCOPY

A portion of the ingot was retained for optical and scanning electron microscopy. The sample was ground using silicon carbide paper in a series of steps from 240 to 600 grit. Polishing was completed with six micron followed by one micron diamond paste. A succesful etch for optical microscopy was found to be a 30 second immersion in Keller's reagent (1%HF, 1.5%HCl, 2.5% HNO₃, 95%H₂O).

Optical microscopy at various magnifications was accomplished to identify the microstructure of the material. Verification of these results and an inclusion study was completed by SEM examination. The SEM was also used to investigate particle sizes of the powder used in X-ray diffraction.

C. X-RAY DIFFRACTION

Powder for X-ray diffraction was passed through a U.S. Standard #400 sieve mesh (38 microns). Powder samples were mounted with Acetone using a procedure developed by McCreery and recommended by Klug and Alexander [Ref. 47, pp. 372-373], with some modifications to account for a difference in the type of specimen holder used.

A Phillips XRG 3100 X-ray generator with a copper target was used for XRD, employing a power setting of 30kV and 35mA. Data acquisition was accomplished with a Norelco Data Control and Processor in conjunction with a scintillation type X-ray detector. In the recording of diffraction peak positions for determination of lattice parameters a goniometer scan rate of two degrees per minute was used. Intensity measurements for structure factor determination were performed using a scan rate of one

every eight minutes. The diffraction peaks generated in this manner on strip chart paper were then carefully cut out and weighed as a means of measuring integrated intensities. Cross checking of intensity measurements was effected by comparison to the counter values provided by the Norelco Data Processor.

IV. RESULTS AND DISCUSSION

A. SAMPLE ANALYSIS

1. Observations of Microstructure

The sample ingot was examined to ensure that the homogenization heat treatment had produced single phase γ -TiAl. Optical microscopy showed no presence of any second phase or large inclusions. Surface microcracks were noted which appeared to be due to improper fusing of material upon solidification from the melt. Following the etch immersion the surface was again examined, showing excellent grain boundary relief and again no second phase or large inclusions. A micrograph of the etched specimen at a photo objective of 50X is shown in Figure 13.

An inclusion study was conducted by SEM in conjunction with a Kevex Spectra Analyzer. Out of 100 fields investigated, only six fields revealed any impurities present. All six inclusions examined were of size three microns or less and contained no significant impurities. Spectra analysis showed traces of silicon in four, indicating possible surface residue left over from the silicon carbide grinding process. Nitrides in small amounts were found in the other two inclusions.

B. X-RAY DIFFRACTION RESULTS

A summary of diffraction peak positions and intensity measurements is given in Appendix A. All values of position are recorded as Cu $K\alpha_1$ peaks for resolvable $K\alpha_1/K\alpha_2$

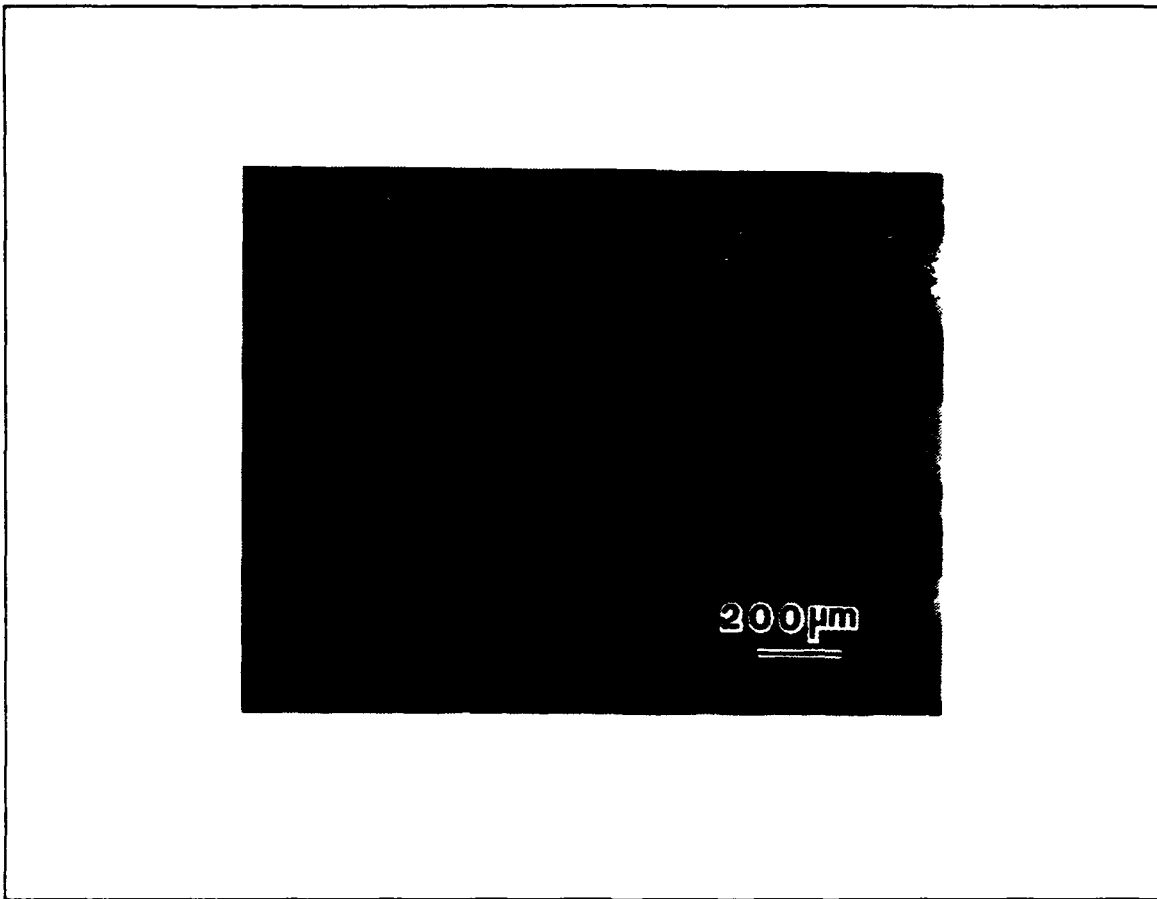


Figure 13. Optical Micrograph of Ti-51at.% Al (50X)

doublets or as $K\alpha$ (weighted average) for those showing no $K\alpha_1/K\alpha_2$ resolution. To ensure the greatest accuracy possible in diffracted intensity measurement, the gain of the strip chart recorder was reset for each reflection so that peak intensities were as close to full scale as possible. The integrated intensities were found by weighing each reflection's paper record of intensity variation using a microbalance capable of measuring to ± 0.1 mg. As expected the (111) reflection produced the largest integrated intensity; all other reflections were scaled to this peak. The relative paper weights for each reflection were then multiplied by a factor of 2×10^6 to arrive at the value of integrated intensity. This

was done to facilitate comparison to the calculated structure factor values in the determination of the Debye-Waller factor by the Wilson Method. Intensity measurements cross-checked quite well with the values obtained from the data processor counting device.

1. Lattice Parameter Measurements

The calculated values based on Bragg's Law for lattice parameters a and c and the corresponding values of the Nelson-Riley function are tabulated in Appendix B for each reflection used in the extrapolation. The (420) reflection was excluded from the analysis of a_o due to its poor differentiation in position from the (402) peak. Because of its low intensity and very broad reflection, peak position for the (003) diffraction was unable to be accurately determined and was excluded from the analysis of c_o .

The extrapolations by least squares fit for a_o and c_o are shown in Figure 14. Lattice parameter values of $a_o = 3.997\text{\AA}$ and $c_o = 4.077\text{\AA}$ were determined, giving a c/a ratio of 1.020. Due to only three data points being available for the c_o extrapolation, its value is less accurate than that of a_o . The linear correlation of the data for a_o was 0.95 while for c_o it was 0.51. Despite this, the results agree favorably with those of Duwez and Taylor; the above values are within 0.2% of their research. [Ref. 20]

The lattice parameters were converted to units of kx and plotted with Duwez and Taylor's original data, as shown in Figure 15 [Ref. 20, p. 71]. The present values are indicated by the square data points. Differences between the current research and Duwez and Taylor's work may be explained by the heat treatments used in each case. The sample used by Duwez and Taylor was quenched from the annealing temperature,

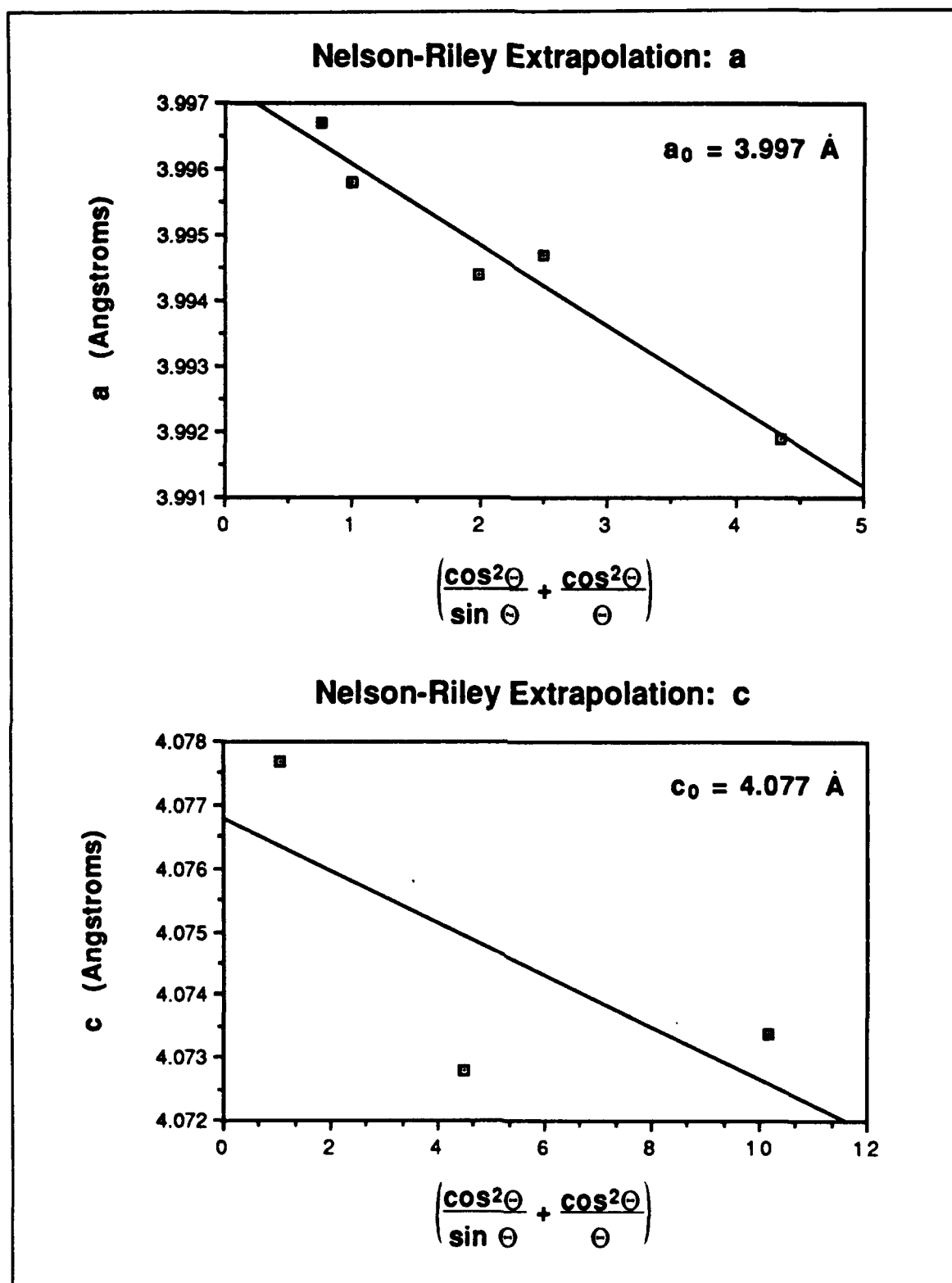
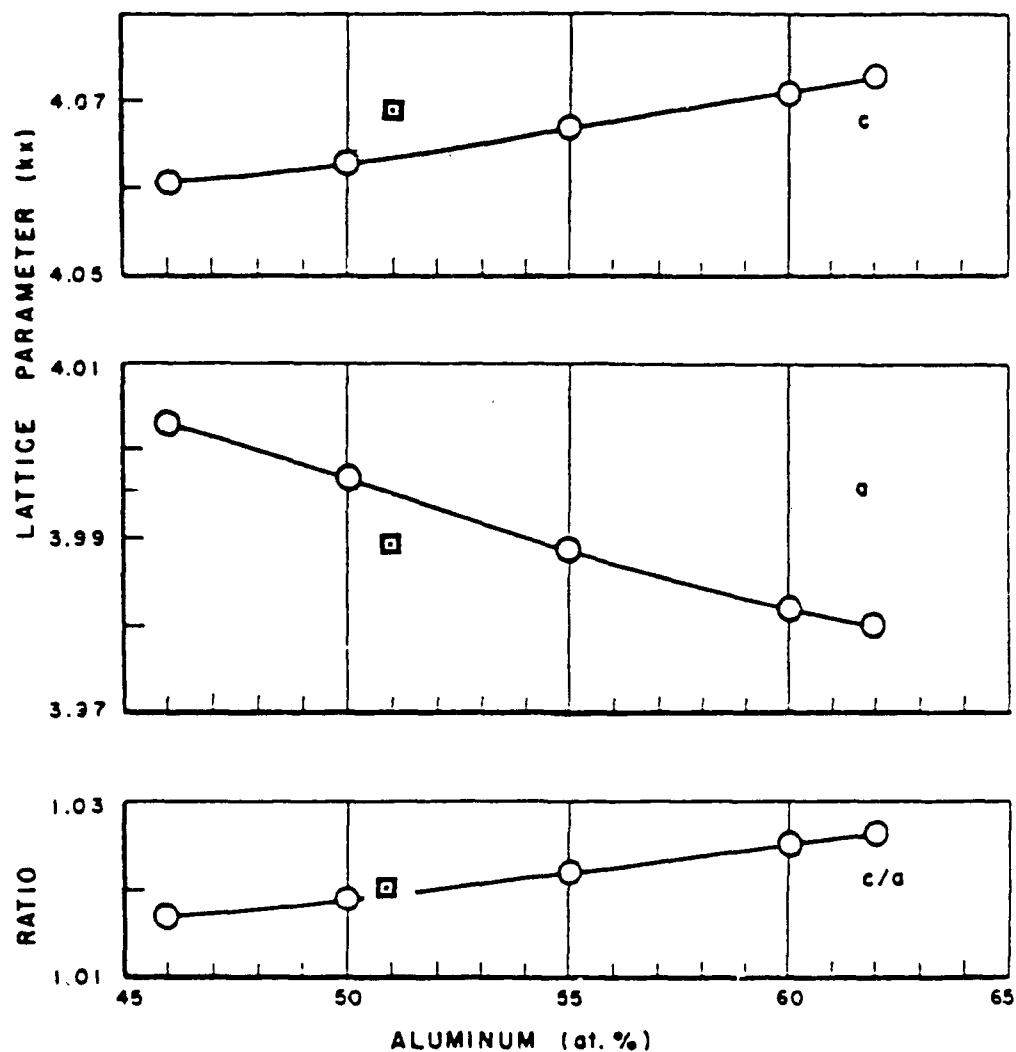


Figure 14. Nelson-Riley Extrapolations for Lattice Parameters a_0 and c_0 .



$$a_0 = 3.997 \text{ \AA}$$

$$c_0 = 4.077 \text{ \AA}$$

$$\frac{c}{a} = 1.020$$

Figure 15. Lattice Parameter Comparison

thereby possibly locking in vacancy defects into the lattice. As previously mentioned, the sample used in this study was allowed to furnace cool following the anneal, avoiding the possibility of large amounts of vacancy defects and increasing the lattice size on average. As a consequence, the c/a ratio found in this study is seen to be slightly larger than Duwez and Taylor's.

2. Measurement of Debye-Waller Factor

A tabulated summary of the data used in calculating Debye-Waller factors for both superlattice and fundamental reflections is given in Appendix C. The values of atomic scattering factor required for theoretical structure factor calculations were obtained using an analytical fit of scattering factor data provided in Volume IV of the *International Tables*. This expression is given as: [Ref. 48, p. 71]

$$f_o\left(\frac{\sin \theta}{\lambda}\right) = \sum_{i=1}^4 a_i \exp\left(-b_i \frac{\sin^2 \theta}{\lambda^2}\right) + c \quad (17)$$

The coefficients a_i , b_i , and c are given for titanium and aluminum in the *International Tables* as well [Ref. 48, p. 99]. Dispersion corrections from the *International Tables* corresponding to Cu $K\alpha$ radiation [Ref. 48, p. 149], [Ref. 52, p. 214] were applied to the values of f_o for each reflection as per Equation (8). The resulting corrected atomic scattering factors were then substituted into Equations (6) and (7) to obtain the respective fundamental and superlattice structure factors.

For the fundamental reflections, a Debye-Waller factor of $B = 0.58 \text{ \AA}^2$ was determined; the curve fit of the data is shown in Figure 16. Due to the extreme effects of extinction at lower Bragg angles, a linear least squares fit was made only on data from

reflections (004) and higher ($\sin \theta/\lambda \geq 0.5$). A correlation value of 0.24 was obtained; this relatively low value is attributed to the reduced number of data points available due to extinction. A significant improvement in accuracy should be possible upon the elimination of extinction and the consequent inclusion of data points for lower angles of reflection.

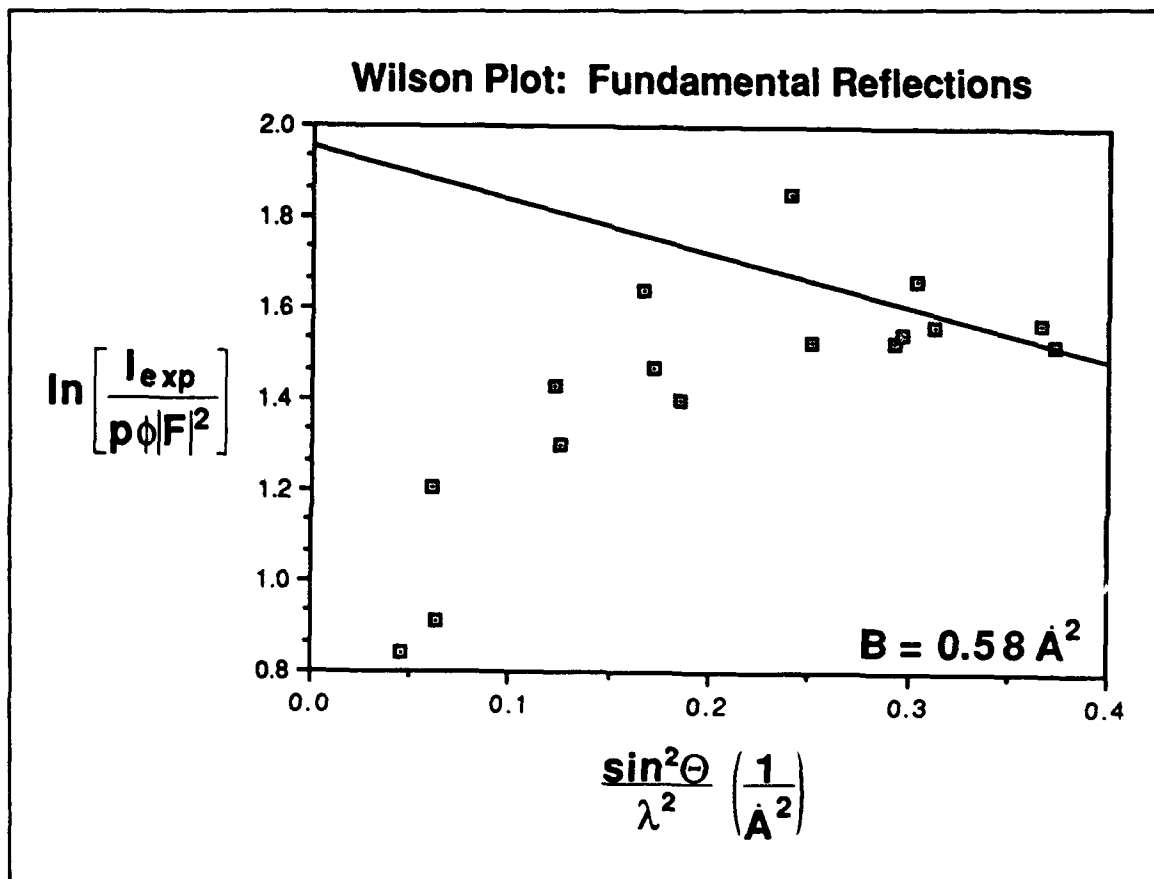


Figure 16. Debye-Waller Determination from Fundamental Reflections

Despite the problems of extinction, the value of $B = 0.58 \text{ \AA}^2$ obtained is deemed to be fairly accurate upon comparison to the characteristic temperature and melting point data. A reasonable approximation can be made of a linear decrease in melting point with increasing aluminum content in the TiAl system. Based on this

approximation and the close agreement between characteristic temperatures of Ti and Al given in the *International Tables*, an average Debye temperature $\Theta = 395$ K was calculated for γ -TiAl. This value was substituted into Equation (11) to obtain a theoretical approximation of $B_{theory} = 0.62 \text{ \AA}^2$.

The superlattice integrated intensities were also affected by extinction, as shown in Figure 17. Due to the low intensities inherent in these reflections, they are more prone to error than fundamental reflections and are an unreliable source of data. Consequently the Debye-Waller factor obtained from the high Bragg angle data points is judged to be inaccurate.

From the observations of the present study there is some question of the validity of the results obtained by Cooper in 1963 [Ref. 2] and Hughes *et al.* in 1971 [Ref. 46] for β' -NiAl. Cooper used powder that was passed through a #400 mesh sieve, while Hughes used a #325 mesh (45 microns). Though Cooper completed a final grinding process on the powder, it is doubtful that this reduced the particle size significantly below 10 to 15 microns. An additional step which he undertook was the compaction of the powder sample, which would most likely introduce more dislocations to the specimen. These dislocations perhaps reduced the effective particle size by disrupting the "mosaic blocks" within the crystals [Ref. 49, p. 140], [Ref. 47, pp. 137-138]. Diffraction line broadening would have been a side effect of this, but a positive outcome perhaps was reduction of extinction effects.

Based on the information shown previously in Figure 12 the results of both Cooper and Hughes *et al.* were likely to be subjected to problems of extinction to one

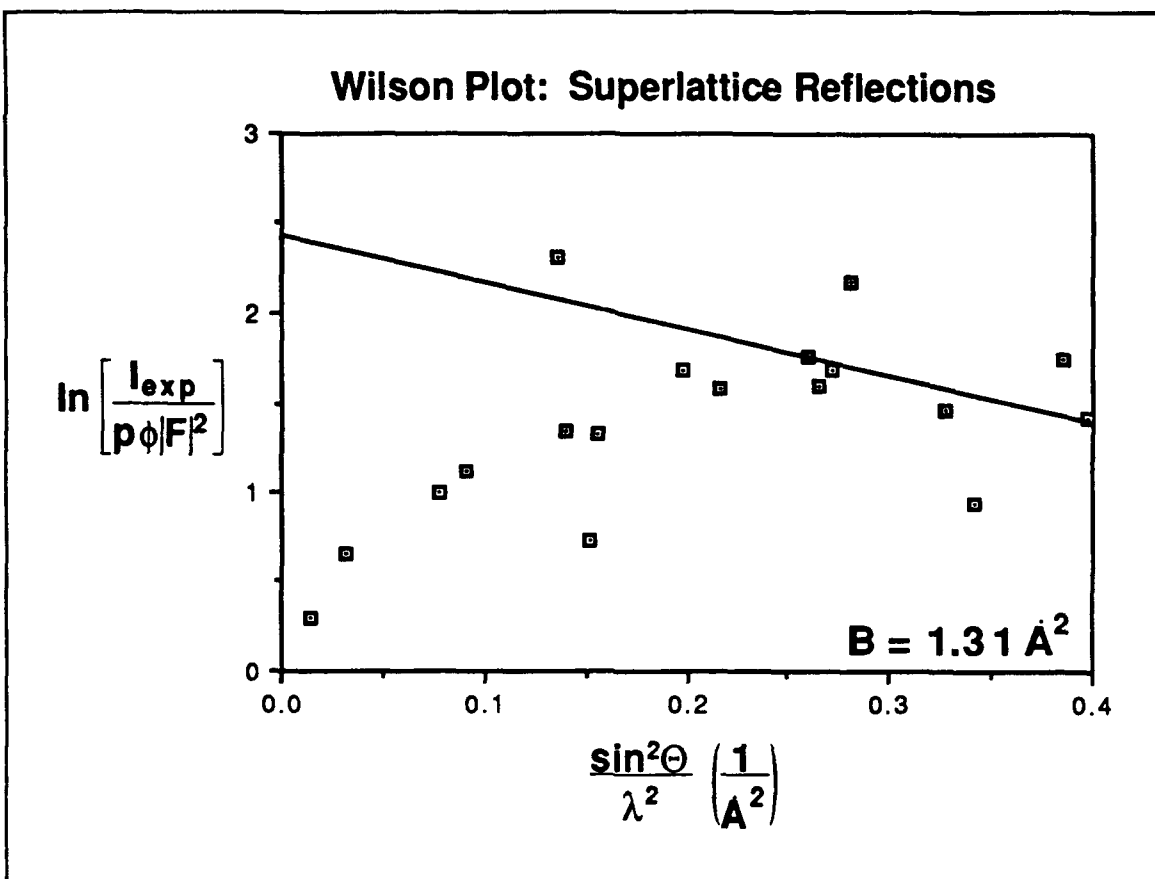


Figure 17. Debye-Waller Determination from Superlattice Reflections

extent or another. Neither of these studies attempted an examination of particle size, though Cooper did not have the luxury of an SEM to complete such an investigation. In addition, the choice of Co $K\alpha$ radiation wavelength by Hughes *et al.* restricted the number of data points available for accurate determination of Debye-Waller factors.

C. PARTICLE SIZE EXAMINATION

An investigation into powder particle size by SEM confirmed the suspected problem of extinction in the X-ray diffraction results. A micrograph at a magnification of 575X is shown in Figure 18; clearly visible are particles approaching the size of the 50 μm bar.

Over 200 particles were randomly measured, resulting in an average particle size of 24.3 μm with a standard deviation of 12.2 μm . Particles as large as 65 μm were found in this investigation.

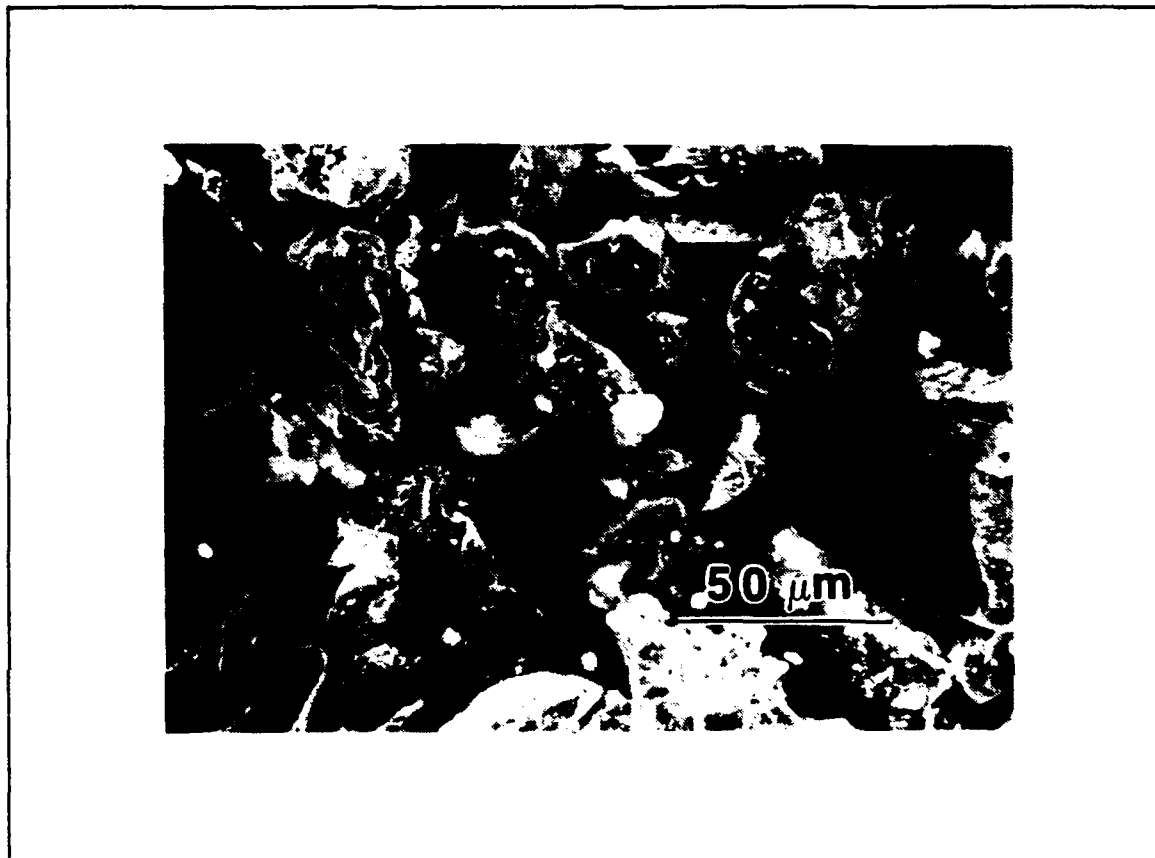


Figure 18. SEM Micrograph of XRD Powder Particles (575X)

Clearly the problem of extinction must be addressed in the measurement of structure factors by X-ray diffraction. Several methods of accounting for extinction effects have been proposed or accomplished. Klug and Alexander have achieved improved results by crushing the powder in a hardened steel mortar and then separating out the smallest particles by sedimentation from methanol [Ref. 47, p. 205-206]. Rotation of the specimen is also recommended by these authors in order to decrease intensity

[Ref. 47, p. 368]. Sabine has endorsed the Rietveld method of data analysis to improve the accuracy of measured intensities subject to extinction and other error problems [Ref. 53]. An interesting process has been developed by Parrish and Hart in which the powder is ground with a hardened sphere and sifted through a Lektromesh screen by acoustic vibration. The mounted specimen is then oscillated during diffraction to achieve the best random orientation of particles [Ref. 54].

V. CONCLUSIONS

This research used powder X-ray diffraction procedures to investigate the lattice structure characteristics of a binary Ti-51at.%Al intermetallic alloy. Included in this study was a verification of previous research on lattice parameters of γ -TiAl, determination of the Debye-Waller temperature factor through accurate measurement of diffracted intensities, and an examination of extinction effects due to XRD powder particle size.

The face-centered tetragonal lattice structure of this alloy was found to have a c/a ratio of 1.020. Unit cell lattice parameters were measured by extrapolation using the Nelson-Riley function; the values of c_0 and a_0 were found to be 4.077Å and 3.997Å respectively. These results agreed with previous data determined by Debye-Scherrer camera methods.

The Debye-Waller temperature factor was determined from fundamental lattice reflections to have a value of $B = 0.58\text{\AA}^2$. Comparison with a theoretical value based on characteristic temperatures and melting point data of titanium and aluminum indicated that this value is reasonably accurate despite problems with extinction at low Bragg angles. Superlattice reflections yielded low levels of diffracted intensity and therefore were subject to greater error in measurement. The Debye-Waller factor determined from superlattice data was considered to be inaccurate for this reason.

An examination of powder particle size confirmed that extinction was a contributing factor to reduced levels of measured intensities, particularly at low angles of reflection.

Average particle size was 24.3 microns, considerably larger than desired for accurate structure factor measurement. Additional research is necessary to investigate methods of minimizing extinction effects through a reduction in crystallite size of X-ray diffraction specimens.

VI. RECOMMENDATIONS

The following suggestions are provided for additional research into TiAl alloys and the determination of bonding characteristics by X-ray diffraction methods:

- To combat the problems of extinction a critical analysis of present procedures and the development of new methods to reduce XRD powder particle size is required. Improved accuracy in structure factor measurement by X-ray diffraction would be a potential benefit of such a study.
- Other methods of structure factor determination--e.g., critical voltage electron diffraction--are available and should be applied to facilitate a better understanding of bonding mechanisms in TiAl. This should include a verification of the Debye-Waller temperature factor determined in the present work.
- Charge density mapping by computer generation using the results of the present research should be attempted. This may provide at least a preliminary observation of electron charge density distribution in γ -TiAl.
- Improvements in the accuracy of intensity measurements can be obtained through the use of a step-scanning goniometer in conjunction with a computerized data acquisition system. The experiments conducted in the present study should be repeated using this equipment.
- Some doubt exists in the location of phase boundaries at high temperature in the titanium-aluminum system. Further research should be conducted to firmly establish the microstructural characteristics of TiAl.

APPENDIX A. XRD REFLECTIONS AND INTEGRATED INTENSITIES

Table 2. REFLECTION POSITIONS AND INTEGRATED INTENSITIES

Reflection (hkl)	Peak Position (degrees 2 θ)	Experimental Intensity (counts)
001	21.83	35900
110	31.68	37220
111	38.76	708000
002	44.43	169300
200	45.38	235800
201	50.86	24400
112	55.56	20080
202	65.34	245200
220	66.08	103600
003	69.21	7430
221	70.48	10530
103	73.84	4850
130	75.10	8420
113	77.93	175400
131	79.29	282200
222	83.09	115900
203	86.56	8126
132	91.65	13330

Table 2. (CONTINUED)

Reflection (hkl)	Peak Position (degrees 2 θ)	Experimental Intensity (counts)
004	98.14	33180
400	100.86	46820
223	103.66	7166
401	105.09	6150
114	106.88	6756
330	109.69	5566
313	112.66	180300
331	114.09	92300
204	116.05	105200
402	118.30	194800 *
420	119.08	
421	123.86	13140
332	128.56	4306
224	137.08	128400
422	140.49	263400
403	146.21	15770
314	152.33	28360

* Intensities for reflections (402) and (420) combined due to overlapping peaks.

APPENDIX B. NELSON-RILEY EXTRAPOLATION DATA

Table 3. NELSON-RILEY EXTRAPOLATION DATA: a

Reflection (hkl)	θ (degrees)	Value of Nelson-Riley Function	a (Å)
200	27.70	4.3536	3.9919
220	33.05	2.5062	3.9947
130	37.58	1.9879	3.9944
400	50.45	0.9863	3.9958
330	54.85	0.7516	3.9967

Table 4. NELSON-RILEY EXTRAPOLATION DATA: c

Reflection (hkl)	θ (degrees)	Value of Nelson-Riley Function	c (Å)
001	10.90	10.1678	4.0734
002	22.23	4.4747	4.0728
004	49.08	1.0689	4.0777

APPENDIX C. WILSON PLOT DATA

Table 5. WILSON PLOT DATA: FUNDAMENTAL REFLECTIONS

Reflection (hkl)	$(\sin \theta/\lambda)^2$ (\AA^{-2})	$p\phi(\theta)F^2$ (counts)	I_{exp} (counts)	$\ln I' *$
111	0.0463	305600	708000	0.8403
002	0.0602	50550	169300	1.2087
200	0.0626	94720	235800	0.9121
202	0.1227	58750	245200	1.4287
220	0.1253	28270	103600	1.2989
113	0.1667	34040	175400	1.6394
131	0.1718	64720	282200	1.4725
222	0.1855	28600	115900	1.3990
004	0.2405	5206	33180	1.8521
400	0.2505	10120	46820	1.5321
313	0.2920	39160	180300	1.5268
331	0.2969	19680	92300	1.5454
204	0.3032	19870	105200	1.6667
402/420	0.3121	40750	194800	1.5647
224	0.3659	26720	128400	1.5696
422	0.3733	57270	263400	1.5259

* $\ln I' = \ln (I_{\text{exp}}/p\phi(\theta)F^2)$ as per the Wilson Method.

Table 6. WILSON PLOT DATA: SUPERLATTICE REFLECTIONS

Reflection (hkl)	$(\sin \theta/\lambda)^2$ (\AA^{-2})	$p\phi(\theta)F^2$ (counts)	I_{exp} (counts)	$\ln I'$
001	0.0150	26580	35900	0.3007
110	0.0314	19340	37220	0.6545
201	0.0775	8981	24400	0.9995
112	0.0914	6518	20080	1.1252
003	0.1356	733	7430	2.3161
221	0.1402	2745	10530	1.3441
103	0.1518	2351	4850	0.7241
130	0.1564	2225	8420	1.3309
203	0.1980	1515	8126	1.6797
132	0.2166	2732	13330	1.5850
223	0.2604	1240	7166	1.7542
401	0.2655	1241	6150	1.6005
114	0.2718	1247	6756	1.6897
330	0.2817	633	5566	2.1740
421	0.3276	3046	13140	1.4618
332	0.3420	1680	4306	0.9412
403	0.3858	2737	15770	1.7512
314	0.3971	6848	28360	1.4210

LIST OF REFERENCES

1. Khataee, A., Flower, H. M., and West, D. R. F., "New Titanium-Aluminum-X Alloys for Aerospace Applications", *Journal of Materials Engineering*, Vol. 10, No. 1, pp. 37-44, 1988.
2. Cooper, M. J., "The Electron Distribution in the Phases CoAl and NiAl", *Philosophical Magazine*, Vol. 8, pp. 811-821, 1963.
3. Fox, A. G., and Tabbernor, M. A., "The Bonding Charge Density of β' NiAl", *Acta Metallurgica*, Vol. 39, No. 4, pp. 669-678, 1991.
4. Khataee, A., Flower, H. M., and West, D. R. F., "The Alloying of Titanium Aluminides with Ruthenium", *Platinum Metals Review*, Vol. 33, No. 3, pp. 106-113, 1989.
5. Sundaresan, R. and Froes, F. H., "Titanium Intermetallics Development Through Mechanical Alloying", *Metal Powder Report*, Vol. 44, No. 3, pp. 206-208, 1989.
6. Benn, R. C., Mirchandani, P. K., and Watwe, A. S., "Intermetallic Systems Produced by Mechanical Alloying", *Proceedings of the 1988 International Powder Metallurgy Conference*, Vol. 21, pp. 479-493, American Powder Metallurgy Institute, 1988.
7. Court, S. A., Vasudevan, V. K., and Fraser, H. L., "Deformation Mechanisms in the Intermetallic Compound TiAl", *Philosophical Magazine A*, Vol. 61, No. 1, pp. 141-158, 1990.
8. Hug, G., Loiseau, A., and Lasalmonie, A., "Nature and Dissociation of the Dislocations in TiAl Deformed at Room Temperature", *Philosophical Magazine A*, Vol. 54, No. 1, pp. 47-65, 1986.
9. McCullough, C., Valencia, J. J., Levi, C. G., and Mehrabian, R., "Phase Equilibria and Solidification in Ti-Al Alloys", *Acta Metallurgica*, Vol. 37, No. 5, pp. 1321-1336, 1989.
10. Sircar, Subhasish, *Phase Transitions in High Temperature Ordered Intermetallic Titanium Aluminum Alloys*, Ph.D. Dissertation, Michigan State University, 1987.

11. Graves, J. A., and Ghosh, A. K., "Microstructure and Elevated Temperature Flow Properties of Rapidly Solidified TiAl-Base Alloys", *Proceedings of the Third Symposium on High-Temperature Ordered Intermetallic Alloys*, pp. 317-322, Materials Research Society, 1989.
12. Konitzer, D. G., Jones, I. P., and Fraser, H. L., "Site Occupancy in Solid Solutions of Nb in the Intermetallic Compounds TiAl and Ti₃Al", *Scripta Metallurgica*, Vol. 20, No. 2, pp. 265-268, 1986.
13. Lipsitt, H. A., "Titanium Aluminides--An Overview", *Materials Research Society Symposium Proceedings*, Vol. 39, pp. 351-364, 1985.
14. Ogden, H. R., Maykuth, D. J., Finlay, W. L., and Jaffee, R. I., "Constitution of Titanium-Aluminum Alloys", *Transactions AIME*, Vol. 191, pp. 1150-1155, 1951.
15. Murray, J. L., in *Binary Alloy Phase Diagrams*, Vol. 1, pp. 225-227, ASM International, 1990.
16. Shull, R. D., McAlister, A. J., and Reno, R. C., "Phase Equilibria in the Titanium-Aluminum System", *Proceedings of the Fifth International Conference on Titanium*, Vol. 3, pp. 1459-1466, 1985.
17. Murray, J. L., "Calculation of the Titanium-Aluminum Phase Diagram", *Metallurgical Transactions A*, Vol. 19A, pp. 243-247, 1988.
18. McCullough, C., Valencia, J. J., Mateos, H., Levi, C. G., and Mehrabian, R., "The High Temperature α Field in the Titanium-Aluminum Phase Diagram", *Scripta Metallurgica*, Vol. 22, No. 7, pp. 1131-1136, 1988.
19. Valencia, J. J., McCullough, C., Levi, C. G., and Mehrabian, R., "Microstructure Evolution During Conventional and Rapid Solidification of a Ti-50at.%Al Alloy", *Scripta Metallurgica*, Vol. 21, No. 10, pp. 1341-1346, 1987.
20. Duwez, P. and Taylor, J. L., "The Crystal Structure of TiAl", *Transactions AIME*, Vol. 194, pp. 70-71, 1952.
21. Li, Z. X., Li, Z. C., and Whang, S. H., "Long-Range Ordering in Rapidly Quenched Ti-Al Compounds", *Materials Science and Engineering*, Vol. 98, pp. 169-172, 1988.
22. Lipsitt, H. A., Shechtman, D., and Schafrik, R. E., "The Deformation and Fracture of TiAl at Elevated Temperatures", *Metallurgical Transactions A*, Vol. 6A, pp. 1991-1996, 1975.
23. Hug, G., Loiseau, A., and Veyssi re, P., "Weak Beam Observation of a Dissociation Transition in TiAl", *Philosophical Magazine*, Vol. 57, No. 3, pp. 499-523, 1988.

24. Greenberg, B. A., Anisimov, V. I., Gornostirev, Yu. N., and Taluts, G. G., "Possible Factors Affecting the Brittleness of the Intermetallic Compound TiAl", *Scripta Metallurgica*, Vol. 22, No. 6, pp. 859-864, 1988.
25. Shechtman, D., Blackburn, M. J., and Lipsitt, H. A., "The Plastic Deformation of TiAl", *Metallurgical Transactions*, Vol 5., No. 6, pp. 1373-1381, 1974.
26. Feng, Hx. R., Michel, D. J., and Crowe, C. R., "Twin Relationships in TiAl", *Scripta Metallurgica*, Vol. 22, pp. 1481-1486, 1988.
27. Feng, C. R., Michel, D. J., and Crowe, C. R., "Twinning in TiAl", *Scripta Metallurgica*, Vol. 23, pp. 1135-1140, 1989.
28. Hanamura, T., and Tanino, M., "A New Type of Twinning in TiAl-2wt.%Mn Intermetallic Compound", *Journal of Materials Science Letters*, Vol. 8, pp. 24-28, 1989.
29. Bumps, E. S., Kessler, H. D., and Hansen, M., "Titanium Aluminum System", *Transactions AIME*, Vol. 194, pp. 609-614, 1952.
30. Huang, S. C., and Hall, E. L., "Plastic Deformation and Fracture of Binary TiAl-Base Alloys", *Metallurgical Transactions A*, Vol. 22A, No. 2, pp. 427-438, 1991.
31. Shong, D. S., and Kim, Y. W., "Discontinuous Coarsening of High Perfection Lamellae in Titanium Aluminides", *Scripta Metallurgica*, Vol. 23, No. 2, pp. 257-261, 1989.
32. Gertsman, V. Yu., Gayanov, R. M., Notkin, A. B., Valiev, R. Z., "Investigation of Grain Boundaries in the TiAl Intermetallic Compound", *Scripta Metallurgica*, Vol. 24, No. 6, pp. 1027-1032, 1990.
33. Schwartz, D. S., and Sastry, S. M. L., "Twin and Fault Structures in Titanium Aluminides", *Scripta Metallurgica*, Vol. 23, No. 9, pp. 1621-1626, 1989.
34. Shih, D. S., Scarr, G. K., and Chesnutt, J. C., "On Microstructural Evolution in Gas Atomized Ti-50at.%Al-2at.%Nb Powder", *Materials Research Society Symposium Proceedings*, Vol. 133, pp. 167-172, 1989.
35. Ren, Y., Chen, G., and Oliver, B. F., "Determination of the Lattice Site Location of Ga in TiAl", *Scripta Metallurgica*, Vol. 25, No. 1, pp. 249-254, 1991.
36. Kad, B. and Oliver, B. F., *Materials Research Society Symposium Proceedings*, Vol. 133, pp. 237-242, 1989.

37. Hug, G., and Veyssi re, P., "TEM Investigation of Dislocations Substructures and Micro Twins in Manganese-Doped TiAl", *International Symposium on Electron Microscopy in Plasticity and Fracture Research of Materials, Dresden, GDR, 8-13 October 1989*, pp. 1-9, 1989.
38. Singh, S. R., and Howe, J. M., "Effect of Ta on Twinning in TiAl", *Scripta Metallurgica*, Vol. 25, No. 2, pp. 485-490, 1991.
39. Feng, C. R., Michel, D. J., and Crowe, C. R., "Microstructures of XDTM Titanium Aluminide at Elevated Temperatures", *Scripta Metallurgica*, Vol. 24, No. 7, pp. 1297-1301, 1990.
40. Feng, C. R., Michel, D. J., and Crowe, C. R., "The Effects of Boron in TiAl/Ti₃Al", *Scripta Metallurgica*, Vol. 23, No. 10, pp. 1707-1712, 1989.
41. Saito, K. and Matsushima, T., "Nitrogen Ion Implantation into the Intermetallic Compound TiAl", *Materials Science and Engineering A*, Vol. 115, pp. 355-359, 1989.
42. Hong, T., Watson-Yang, T. J., Guo, X.-Q., Freeman, A. J., Oguchi, T., and Xu, J., "Crystal Structure, Phase Stability, and Electronic Structure of Ti-Al Intermetallics: Ti₃Al", *Physical Review B*, Vol. 43, No. 3, pp. 1940-1947, 1991.
43. Takama, T., and Sato, S., "Accurate Determination of Structure Factors by Pendell sung Methods using White Radiation", *Australian Journal of Physics*, Vol. 41, pp. 433-448, 1988.
44. Fox, A. G., and Fisher, R. M., "A Summary of Low-angle X-ray Atomic Scattering Factors Measured by the Critical Voltage Effect in High Energy Electron Diffraction", *Australian Journal of Physics*, Vol. 41, pp. 461-468, 1991.
45. Shirley, C. G., Lally, J. S., Thomas, L. E., and Fisher, R. M., "High-Voltage Electron Diffraction Measurement of the Debye Temperatures of Cr, α -Fe and their Disordered Alloys", *Acta Crystallographica*, Vol. A31, pp. 174-177, 1975.
46. Hughes, T., Lautenschlager, E. P., Cohen, J. B., and Brittain, J. O., "X-Ray Diffraction Investigation of β' -NiAl Alloys", *Journal of Applied Physics*, Vol. 42, No. 10, pp. 3705-3716, 1971.
47. Klug, H. P., and Alexander, L. E., *X-Ray Diffraction Procedures*, 2nd ed., John Wiley & Sons, 1974.
48. *International Tables For X-Ray Crystallography*, Vol. 4, pp. 45-151, The Kynoch Press, 1974.

49. Cullity, B. D., *Elements of X-Ray Diffraction*, 2nd ed., Addison-Wesley, 1978.
50. *International Tables for X-Ray Crystallography*, Vol. II, pp. 241-265, Kynoch Press, 1959.
51. *International Tables for X-Ray Crystallography*, Vol. III, pp. 232-244, 1962.
52. *International Tables for X-Ray Crystallography*, Vol. III, The Kynoch Press, 1962.
53. Sabine, T. M., "Accurate Structure Factor Measurements by Powder Methods", *Australian Journal of Physics*, Vol. 41, pp. 413-422, 1988.
54. Parrish, W., and Hart, M., "Accurate Measurement of Powder Diffraction Intensities Using Synchrotron Radiation", *Australian Journal of Physics*, Vol. 41, pp. 403-411, 1988.

INITIAL DISTRIBUTION LIST

	No. Copies
1. Defense Technical Information Center Cameron Station Alexandria, VA 22304-6145	2
2. Library, Code 52 Naval Postgraduate School Monterey, CA 93943-5002	2
3. Department Chairman, Code ME/Hy Department of Mechanical Engineering Naval Postgraduate School Monterey, CA 93943-5000	1
4. Weapons Engineering Curricular Office, Code 33 Naval Postgraduate School Monterey, CA 93943-5000	1
5. Professor Terry R. McNelley, Code ME/Mc Department of Mechanical Engineering Naval Postgraduate School Monterey, CA 93943-5000	1
6. Dr. Alan G. Fox, Code ME/Fx Department of Mechanical Engineering Naval Postgraduate School Monterey, CA 93943-5000	2
7. LT Steven C. Cade, USN 9040 Foxhunter Lane Cincinnati, OH 45242	2